Univerza
v Ljubljani

Fakulteta
*za gradbeništvo
in geodezijo*
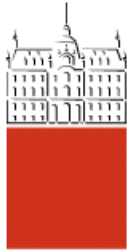
Jamova 2
1000 Ljubljana, Slovenija
http://www3.fgg.uni-lj.si/

DRUGG – Digitalni repozitorij UL FGG
http://drugg.fgg.uni-lj.si/

Ta članek je avtorjeva zadnja recenzirana različica, kot je bila sprejeta po opravljeni recenziji.

Prosimo, da se pri navajanju sklicujte na bibliografske podatke, kot je navedeno:

University
of Ljubljana

Faculty of
*Civil and Geodetic
Engineering*

Jamova 2
SI – 1000 Ljubljana, Slovenia
http://www3.fgg.uni-lj.si/

DRUGG – The Digital Repository
http://drugg.fgg.uni-lj.si/

This version of the article is author's manuscript as accepted for publishing after the review process.

When citing, please refer to the publisher's bibliographic information as follows:

Multilayered shell finite element with interlaminar continuous shear stresses: a refinement of the Reissner-Mindlin formulation

Boštjan Brank [1] and Erasmo Carrera[2]

[1] *Slovenian National Building and Civil Engineering Institute, Dimiceva 12, Ljubljana and Faculty of Civil Engineering and Geodesy, University of Ljubljana, Jamova 2, Ljubljana, Slovenia*

[2] *Department of Aeronautics and Aerospace Engineering, Politecnico di Torino, Corso Duca degli Abruzzi 24, Torino, Italy*

SUMMARY

A finite element formulation for refined linear analysis of multilayered shell structures of moderate thickness is presented. An underlying shell model is a direct extension of the first-order shear-deformation theory of Reissner-Mindlin type. A refined theory with seven unknown kinematic fields is developed: (i) by introducing an assumption of a zig-zag (i.e. layer-wise linear) variation of displacement field through the thickness, and (ii) by assuming an independent transverse shear stress fields in each layer in the framework of Reissner's mixed variational principle. The introduced transverse shear stress unknowns are eliminated on the cross-section level. At this process, the interlaminar equilibrium conditions (i.e. the interlaminar shear stress continuity conditions) are imposed. As a result, the weak form of constitutive equations (the so-called weak form of Hooke's law) is obtained for the transverse strains-transverse stress resultants relation. A finite element approximation is based on the four-noded isoparametric element. To eliminate the shear locking effect, the assumed strain variational concept is used. Performance of the derived finite element is illustrated with some numerical examples. The results are compared with the exact three-dimensional solutions, as well as with analytical and numerical solutions obtained by the classical, the first-order and some representative refined models.

Key words: multilayered shells, FEM, interlaminar equilibrium, mixed methods, Reissner-Mindlin

1. INTRODUCTION

In the recent years, a considerable attention has been paid to the development of models that can accurately describe a response of thicker multilayered anisotropic shells. Design of (moderately) thick multilayered shell component namely requires an accurate prediction of local stress and strain fields in order to locate regions where damage is likely to occur. As experienced by three-dimensional (3D) elasticity solutions (e.g. References [1-3]), a variation of mechanical

properties in the thickness direction leads to the following phenomena: Displacement and transverse stress fields are continuous through the thickness, but they have discontinuous derivatives (with respect to the through-thickness co-ordinate) at layer interfaces. This is often called a *zig-zag* form of displacements and an *interlaminar continuity* of transverse stresses (see e.g. References [4, 5]).

Since 3D analytical solutions for multilayered structural problems are limited (mainly to linear problems with simple geometry and specific stacking-sequences), a number of two-dimensional plate and shell models have been developed during the last three decades. They may be roughly grouped into the classical lamination theories (CLT), the first-order shear-deformation theories (FSDT) and the refined or the higher-order shear-deformation theories (HSDT); as well as into the layer-wise models (LWM) and the equivalent single-layer models (ESLM)—depending on whether or not the number of the unknown variables is related to the number of constitutive layers. Classical LWM were proposed e.g. by Srinivas [6], refined LWM models were developed e.g. by Reddy [7] and a mixed LWM was recently presented by Carrera [8]. Relevant ESLM contributions were reported e.g. by Ren [9] and Murakami [10]. Overviews on the two-dimensional modelling of multilayered structures may be found in review papers (see e.g. References [11–14]). The main conclusions which emerge from those publications are: (i) For higher h/L ratio (h is shell thickness and L is its representative span) and for higher lamina orthotropic ratio E_L/E_T (E_L and E_T are longitudinal and transverse elastic moduli of the lamina, respectively) the CLT analysis may be inadequate to predict the *overall response* of the laminate; FSDT analysis is required for such cases. (ii) FSDT analysis cannot describe the above-mentioned zig-zag and the interlaminar continuity effects; therefore refined models, such as HSDT, are required to predict the *local state* of displacements and stresses. (iii) Accurate evaluations of transverse normal stresses and related effects demand the use of LWM.

Many multilayered plate and shell finite elements have been proposed on the basis of classical or refined models (see e.g. References [7, 15–17]). On the side of finite element formulations based on ESLM, relevant contributions were given e.g. by Basar *et al.* [18] and Di and Ramm [19] (who developed ESLM hybrid finite elements). LWM-based finite element formulations were presented e.g. by Pinsky and Kim [20], Braun *et al.* [21], Basar *et al.* [18] and Gruttmann *et al.* [22], among others.

In this work we focus on the development of a relatively simple refined theory for multilayered shell (and its efficient finite element implementation) which takes into account the above-mentioned zig-zag and interlaminar continuity effects (also named C_z^0-requirements in the terminology of Carrera [4, 5]). The model may be regarded as a *direct extension* (refinement) of the FSDT of Reissner–Mindlin type. The attention is therefore restricted to the ESLM. The transverse normal stress is not included into the theory. The obtained shell finite elements are denoted as RMZC (Reissner–Mindlin zig-zag continuity).

The fundamental tool used in the present developments is the Reissner's mixed variational principle [23], which permits an assumption of two independent fields through the shell thickness, namely the displacement field and the transverse shear stress field. The introduced shear stress unknown variables are eliminated on the cross-section level. Displacement-based formulation with *seven degress-of-freedom per node* is obtained, along with the weak form of the transverse shear constitutive relations (the so-called weak form of Hooke's law). The same approach was successfully used for plates in References [24, 25]. It should be noted, that the RMZC formulation introduced *only* the transverse shear stresses in the framework of the Reissner's variational principle. Therefore, there is no need for condensation of stress variables at the element

level as in Reference [19]. Transverse shear stresses are computed *a priori*, i.e. they are not recovered at a post-processing level via an integration of the 3D indefinite equilibrium equations.

The paper is organized as follows: basic relations of the present refined shell model are presented in Section 2; Section 3 defines mixed functional which is the governing equation for the finite element approximation in Section 5; elimination of stress variables on the cross-section level, enforcement of interlaminar shear stress continuity and derivation of the so-called weak form of Hooke's law is described in detail in Section 4; numerical examples are presented in Section 6 and the main conclusions are drawn in Section 7.

2. BASIC MECHANICS OF THE MODEL

2.1. Geometry

Let us define a geometry of a multilayered shell, composed of N_{lay} layers of composite materials, as

$$\mathbf{X} = \mathbf{X}^0 + \xi \mathbf{T} \tag{1}$$

where $\mathbf{X}^0$ is the middle surface of the shell and $\mathbf{T}$ is the shell-director (vector) field which is by definition perpendicular to the middle surface. We define the domain of the through-thickness co-ordinate ξ as $\xi \in [-h/2, h/2] = [h^-, h^+]$, where h is the (constant) shell thickness, and set the length of the shell-director field to unity, i.e. $\|\mathbf{T}\| = 1$. We further parameterize the shell middle surface by two curvilinear co-ordinates, ξ^1 and ξ^2, so that $\mathbf{X}^0 = \varphi(\xi^1, \xi^2)$ and $\mathbf{T} = \mathbf{T}(\mathbf{X}^0(\xi^1, \xi^2)) = t(\xi^1, \xi^2)$.

2.2. Displacement field

To approximate the thickness variation of in-plane displacements, a *zig-zag-shaped function* is added to the standard linear variation of displacements through the thickness (i.e. to the Reissner–Mindlin-type of assumed displacements); see Figures 1, 2 and References [10, 24, 26].

The displacement field, $\mathbf{u}$, has now the following form:

$$\mathbf{u} = \mathbf{u}^0 + \xi \mathbf{w} + f(\xi)\mathbf{D} \tag{2}$$

where $\mathbf{u}^0$ is the displacement field of the middle surface, $\mathbf{w}$ is the through-thickness displacement field related to the *rotation* of $\mathbf{T}$, $f(\xi)$ is a layer-dependent zig-zag-shaped function which is at layer $K \in [1, N_{\text{lay}}]$ defined as

$$f(\xi_K) = (-1)^K \frac{\xi_K}{h_K/2} \tag{3}$$

and $\mathbf{D}$ is the displacement field related to the *wrinkling* of the shell cross-sections. The domain of ξ_K co-ordinate is $\xi_K \in [-h_K/2, h_K/2] = [h_K^-, h_K^+]$, where h_K is the thickness of the Kth layer. Relation between the co-ordinates ξ_K and ξ is $\xi = \xi_K + \xi^{K0}$, where ξ^{K0} is the value of ξ at $\xi_K = 0$. In what follows, we assume that layer 1 begins at $\xi = -h/2$.

Deformed position of the shell-director vector at a particular point of the middle surface may be given as $\mathbf{RT}$, where $\mathbf{R}$ is a matrix defining small (infinitesimal) rotation of vector $\mathbf{T}$. Matrix $\mathbf{R}$ does not include a rotation of $\mathbf{T}$ around its axis, and may be therefore defined only by *two*
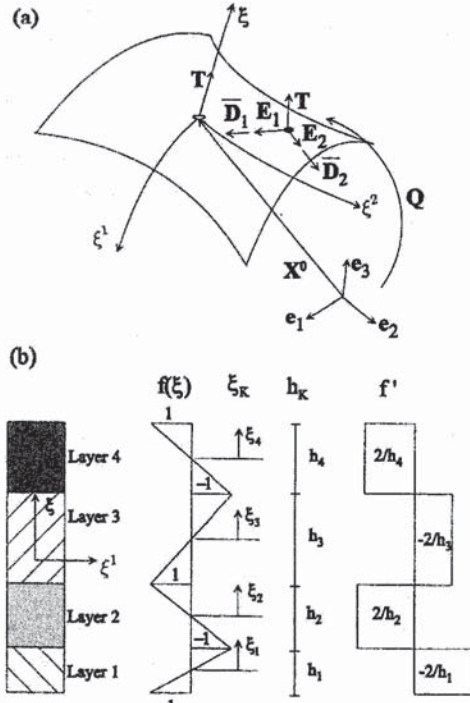
Figure 1. Notation.
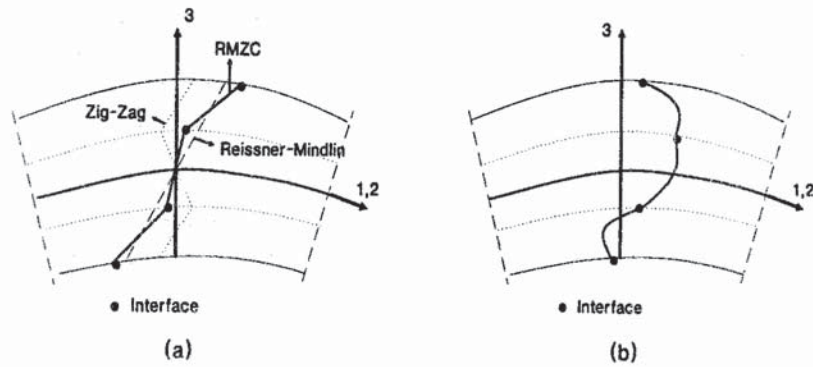
Figure 2. (a) Assumed displacements; and (b) transverse shear stress fields in the thickness direction.

rotational parameters, e.g. α and β. The definition of those two parameters depends upon the chosen description for $\mathbf{R}$ (see e.g. Reference [27] for various possibilities). We may now write the through-thickness displacement field related to the rotation of $\mathbf{T}$ as

$$\mathbf{w} = \mathbf{R}(\alpha, \beta)\mathbf{T} - \mathbf{T} \qquad (4)$$

Since **D** defines the refined through-thickness part of displacements (see (b)), the following constraint has to be satisfied at a particular point of the middle surface:

$$\mathbf{D} \cdot \mathbf{T} = 0 \tag{5}$$

Due to restriction (5), only *two* components of vector **D** are independent. In this sense it is suitable to define at a particular point of the middle surface an orthonormal local co-ordinate with base vectors $\{\mathbf{E}_i\}$, which are oriented such that $\mathbf{E}_3 = \mathbf{T}$. Vectors $\mathbf{E}_1$ and $\mathbf{E}_2$ then lie on the tangent plane to the middle surface at the considered point. Triad $\{\mathbf{E}_i\}$ may be expressed with base vectors $\{\mathbf{e}_i\}$ of fixed (global) orthonormal co-ordinate system as $\mathbf{E}_i = \mathbf{Q}\mathbf{e}_i$, where $\mathbf{Q} = [\mathbf{E}_1, \mathbf{E}_2, \mathbf{E}_3]_{(3\times3)}$ is an orthogonal matrix. We denote the three components of vector **D**, related to the global co-ordinate system, as D_i. Similarly, we denote the three components of vector **D**, related to the local co-ordinate system, as $\widetilde{D}_i$ (see Figure 1). By noting that $\widetilde{D}_3 = 0$, and using standard transformation relations, we have

$$\begin{Bmatrix} D_1 \\ D_2 \\ D_3 \end{Bmatrix} = \widetilde{\mathbf{Q}} \begin{Bmatrix} \widetilde{D}_1 \\ \widetilde{D}_2 \end{Bmatrix}, \quad \widetilde{\mathbf{Q}} = [\mathbf{E}_1, \mathbf{E}_2]_{(3\times2)} \tag{6}$$

Note, that $\widetilde{D}_1$ has a direction of $\mathbf{E}_1$, while $\widetilde{D}_2$ has a direction of $\mathbf{E}_2$. With (b), (4) and (6) we obtain *seven* unknown displacement degrees of freedom at each middle surface point. By collecting them in a generalized displacement vector, we have

$$\mathbf{U} = \{u_1^0, u_2^0, u_3^0, \alpha, \beta, \widetilde{D}_1, \widetilde{D}_2\}^{\mathrm{T}} \tag{7}$$

where $\mathbf{u}^0 = u_i^0 \mathbf{e}_i$.

2.3. Transverse shear stress fields

A mixed variational principle, which is introduced below in Section 3.2, allows us to make an assumption of independent transverse shear stress fields at each layer. In this work we assume that the transverse shear stresses vary *quadratically* through the layers. We may then write (see Figure 2) for a layer $K \in [1, N_{\mathrm{lay}}]$

$$\sigma_K^{\alpha3} = \sigma_K^{\alpha3,\mathrm{top}} F_0 + R_K^{\alpha3} F_1 + \sigma_K^{\alpha3,\mathrm{bot}} F_2 \tag{8}$$

where the superscripts top and bot refer to the top (at $\xi_K = h_K/2$) and bottom (at $\xi_K = -h_K/2$) edges of the layer, respectively. $R_K^{\alpha3}$ are layer stress resultants defined as

$$R_K^{\alpha3} = \int_{h_K^-}^{h_K^+} \sigma_K^{\alpha3} \mu \, \mathrm{d}\xi_K \tag{9}$$

while functions F_i, $i = 0, 1, 2$, have the following forms:

$$F_0 = -\frac{1}{4} + \frac{\zeta_K}{2} + \frac{3}{4}\zeta_K^2, \quad F_1 = \frac{3(1 - \zeta_K^2)}{2h_K}, \quad F_2 = -\frac{1}{4} - \frac{\zeta_K}{2} + \frac{3}{4}\zeta_K^2 \tag{10}$$

where co-ordinate ζ_K is defined as $\zeta_K = \xi_K/(h_K/2)$, therefore $\zeta_K \in [-1, 1]$. By introducing a vector of unknown stress parameters, χ_K, and a vector of assumed transverse shear stresses, σ_K,

$$\chi_K = \{\sigma_K^{13,\mathrm{top}}, \sigma_K^{23,\mathrm{top}}, R_K^{13}, R_K^{23}, \sigma_K^{13,\mathrm{bot}}, \sigma_K^{23,\mathrm{bot}}\}^{\mathrm{T}}, \quad \sigma_K = \{\sigma_K^{13}, \sigma_K^{23}\}^{\mathrm{T}} \tag{11}$$

Equation (8) may be rewritten in more compact notation as

$$\sigma_K = \mathbf{E}\,\chi_K \tag{12}$$

where

$$\mathbf{E} = \begin{bmatrix} F_0 & 0 & F_1 & 0 & F_2 & 0 \\ 0 & F_0 & 0 & F_1 & 0 & F_2 \end{bmatrix} \tag{13}$$

For later use we integrate (13) through the thickness of a layer. From relations

$$\int_{h_K^-}^{h_K^+} F_0\,\mu\,\mathrm{d}\xi_K \overset{\mu=1}{=} 0, \qquad \int_{h_K^-}^{h_K^+} F_2\,\mu\,\mathrm{d}\xi_K \overset{\mu=1}{=} 0, \qquad \int_{h_K^-}^{h_K^+} F_1\,\mu\,\mathrm{d}\xi_K \overset{\mu=1}{=} 1 \tag{14}$$

it follows that the resulting matrix has a simple form

$$\int_{h_K^-}^{h_K^+} \mathbf{E}\,\mu\,\mathrm{d}\xi_K \overset{\mu=1}{=} \begin{bmatrix} 0 & 0 & 1 & 0 & 0 & 0 \\ 0 & 0 & 0 & 1 & 0 & 0 \end{bmatrix} \tag{15}$$

The geometric quantity μ is defined by $\mathrm{d}V = \mathrm{d}S\,\mu\,\mathrm{d}\xi$, where $\mathrm{d}V$ is a volume differential of the shell and $\mathrm{d}S$ is an area differential of the middle surface. When $\mu = 1$, a variation of metrics through the thickness of a laminate is neglected.

2.4. Strain measures

The Green–Lagrange strain measures are defined as the difference of metric tensors of the deformed and undeformed configurations at the same material point. Linear strain measures may be obtained by evaluating the metric tensors (using (1) and (b)) and by further neglecting the non-linear terms. For the present model we obtain the following expressions:

$$E_{\alpha\beta} = \tfrac{1}{2}(\mathbf{X}_{,\alpha}^0 \cdot \mathbf{u}_{,\beta}^0 + \mathbf{X}_{,\beta}^0 \cdot \mathbf{u}_{,\alpha}^0) + \tfrac{1}{2}\xi[\mathbf{X}_{,\alpha}^0 \cdot \mathbf{w}_{,\beta} + \mathbf{X}_{,\beta}^0 \cdot \mathbf{w}_{,\alpha}] + \tfrac{1}{2}f(\xi)(\mathbf{X}_{,\alpha}^0 \cdot \mathbf{D}_{,\beta} + \mathbf{X}_{,\beta}^0 \cdot \mathbf{D}_{,\alpha})$$

$$E_{\alpha 3} = \tfrac{1}{2}(\mathbf{X}_{,\alpha}^0 \cdot \mathbf{w}) + \tfrac{1}{2}f'(\mathbf{X}_{,\alpha}^0 \cdot \mathbf{D}) \tag{16}$$

$$E_{33} = 0$$

where $(\circ)_{,\alpha}$ denotes $\partial(\circ)/\partial\xi^\alpha$, while f' is $\mathrm{d}f(\xi)/\mathrm{d}\xi$; for layer K we have

$$f_K' = (-1)^K \frac{2}{h_K} \tag{17}$$

Equations (16) may be also written in a more compact form as

$$E_{\alpha\beta} = \varepsilon_{\alpha\beta} + \xi\kappa_{\alpha\beta} + f(\xi)\kappa_{\alpha\beta}^f$$

$$2E_{\alpha 3} = \gamma_{\alpha 3} + f'\gamma_{\alpha 3}^f \tag{18}$$

Variations of strain measures (16) are

$$\delta E_{\alpha\beta} = \tfrac{1}{2}(\mathbf{X}_{,\alpha}^0 \cdot \delta\mathbf{u}_{,\beta}^0 + \mathbf{X}_{,\beta}^0 \cdot \delta\mathbf{u}_{,\alpha}^0) + \tfrac{1}{2}\xi[\mathbf{X}_{,\alpha}^0 \cdot \delta\mathbf{w}_{,\beta} + \mathbf{X}_{,\beta}^0 \cdot \delta\mathbf{w}_{,\alpha}]$$

$$+ \tfrac{1}{2}f(\xi)(\mathbf{X}_{,\alpha}^0 \cdot \delta\mathbf{D}_{,\beta} + \mathbf{X}_{,\beta}^0 \cdot \delta\mathbf{D}_{,\alpha}) \tag{19}$$

$$\delta E_{\alpha 3} = \tfrac{1}{2}(\mathbf{X}_{,\alpha}^0 \cdot \delta\mathbf{w}) + \tfrac{1}{2}f'(\mathbf{X}_{,\alpha}^0 \cdot \delta\mathbf{D})$$

where (see (4) and (6))

$$\delta \mathbf{w} = \Lambda \left\{ \begin{matrix} \delta\alpha \\ \delta\beta \end{matrix} \right\}, \quad \delta \mathbf{D} = \tilde{\mathbf{Q}} \left\{ \begin{matrix} \delta\tilde{D}_1 \\ \delta\tilde{D}_2 \end{matrix} \right\} \tag{20}$$

with Λ being a (3×2) matrix emerging from the variation of (4). By using the more compact notation introduced in (18), they may read as

$$\begin{aligned} \delta E_{\alpha\beta} &= \delta\varepsilon_{\alpha\beta} + \xi\delta\kappa_{\alpha\beta} + f(\xi)\delta\kappa_{\alpha\beta}^f \\ 2\delta E_{\alpha 3} &= \delta\gamma_{\alpha 3} + f'\delta\gamma_{\alpha 3}^f \end{aligned} \tag{21}$$

2.5. Hooke's law for orthotropic lamina

In this section we work with standard constitutive relations for elastic orthotropic materials (see e.g. Reference [28]). Let us introduce at a material point of layer $K \in [1, N_{\text{lay}}]$ Cartesian co-ordinate system x_i^*. Orientation of x_3^* is such that $x_3^* = \xi + \xi_c$, where ξ_c is a constant. Three-dimensional constitutive relations in these co-ordinates are $\sigma^{ij,*} = H_K^{ijkl,*} E_{ij}^*$. Since $E_{33}^* = E_{33} = 0$, see (16), the stretch in the thickness direction is obtained by assuming that $\sigma^{33,*} = \sigma^{33} = 0$. Three-dimensional constitutive relations may be then condensed as $C_K^{ijkl,*} = H_K^{ijkl,*} - H_K^{33kl,*}/H_K^{3333,*}$, $_{ij \neq 33, kl \neq 33}$ and the stress–strain relations at a given material point may be written in the familiar form

$$\left\{ \begin{matrix} \sigma^{11,*} \\ \sigma^{22,*} \\ \sigma^{12,*} \\ \sigma^{13,*} \\ \sigma^{23,*} \end{matrix} \right\} = \begin{bmatrix} C_K^{1111,*} & C_K^{1122,*} & 0 & 0 & 0 \\ & C_K^{2222,*} & 0 & 0 & 0 \\ & & C_K^{1212,*} & 0 & 0 \\ & & & C_K^{1313,*} & 0 \\ \text{symm.} & & & & C_K^{2323,*} \end{bmatrix} \left\{ \begin{matrix} E_{11}^* \\ E_{22}^* \\ 2E_{12}^* \\ 2E_{13}^* \\ 2E_{23}^* \end{matrix} \right\} \tag{22}$$

Non-zero components of constitutive relations (22) are defined (for orthotropic material) by six independent material parameters which are: two elastic moduli E_1, E_2, three shear moduli G_{12}, G_{13}, G_{23} and one Poisson's ratio $v_{12} = v_{21}E_1/E_2$. (Poisson's ratio is defined as $v_{12} = -E_{11}^*/E_{22}^*$.) Their explicit forms are

$$\begin{aligned} C_K^{1111,*} &= \frac{E_1}{1 - v_{12}^2 E_2/E_1}, & C_K^{2222,*} &= \frac{E_2}{1 - v_{12}^2 E_2/E_1}, & C_K^{1122,*} &= \frac{v_{12}E_2}{1 - v_{12}^2 E_2/E_1} \\ C_K^{1212,*} &= G_{12}, & C_K^{1313,*} &= G_{13}, & C_K^{2323,*} &= G_{23} \end{aligned} \tag{23}$$

In the above notation the subscript 1 relates to the fibre direction (the direction of x_1^*), the subscript 2 relates to the direction transverse to the fibres (the direction of x_2^*) and the subscript 3 is associated with the through-thickness direction defined by co-ordinates x_3^*, ξ_K and ξ. In order to integrate constitutive relations through the thickness of a laminate, these relations need to be transformed to the shell curvilinear co-ordinates. Transformation of the fourth-order tensor from the layer Cartesian co-ordinates x_i^* to the shell curvilinear co-ordinates $\xi^\alpha, \xi^3 = \xi$ is performed in the standard way as

$$C_K^{ijkl} = T_{mi}T_{nj}C_K^{mnop,*}T_{ok}T_{pl}, \quad ij \neq 33, kl \neq 33, mn \neq 33, op \neq 33 \tag{24}$$

where $T_{mi} = \partial\xi^i/\partial x_m^*$. In view of the finite element implementation of the multilayered shell model, the curvilinear shell co-ordinates ξ^α, ξ may be locally replaced by Cartesian co-ordinate system

$\widehat{x}_i$ ($\widehat{x}_1 \equiv \widehat{x}$, $\widehat{x}_2 \equiv \widehat{y}$, $\widehat{x}_3 \equiv \widehat{z}$), such that $\zeta \equiv \widehat{x}_3$. In this case the transformation coefficients T_{mi} take simple form. They may be presented as

$$[T_{mi}] = \begin{bmatrix} \cos\theta & -\sin\theta & 0 \\ \sin\theta & \cos\theta & 0 \\ 0 & 0 & 1 \end{bmatrix} \tag{25}$$

where θ is an angle which rotates x_1^* into $\widehat{x}$ when the positive axis of rotation is defined by $+\widehat{x}_3$. Once transformation (24) is performed, we obtain the following relations with respect to the introduced local Cartesian co-ordinates $\widehat{x}_i$:

$$\begin{Bmatrix} \sigma^{11} \\ \sigma^{22} \\ \sigma^{12} \end{Bmatrix} = \mathbf{C}_K \begin{Bmatrix} E_{11} \\ E_{22} \\ 2E_{12} \end{Bmatrix}, \quad \begin{Bmatrix} \sigma^{13} \\ \sigma^{23} \end{Bmatrix} = \mathbf{C}_K^s \begin{Bmatrix} 2E_{13} \\ 2E_{23} \end{Bmatrix} \tag{26}$$

where

$$\mathbf{C}_K = \begin{bmatrix} \mathbf{C}_K^{1111} & \mathbf{C}_K^{1122} & \mathbf{C}_K^{1112} \\ & \mathbf{C}_K^{2222} & \mathbf{C}_K^{2212} \\ \text{symm.} & & \mathbf{C}_K^{1212} \end{bmatrix}, \quad \mathbf{C}_K^s = \begin{bmatrix} \mathbf{C}_K^{1313} & \mathbf{C}_K^{1323} \\ \text{symm.} & \mathbf{C}_K^{2323} \end{bmatrix} \tag{27}$$

Explicit expressions for $\mathbf{C}_K$ and $\mathbf{C}_K^s$ matrices may be found in standard textbooks on composite laminates (see e.g. Reference [28]).

3. GOVERNING EQUATIONS

Having defined strains, assumed stresses and lamina constitutive relations, we may proceed with virtual work equation and mixed variational equation. The latter represents a starting point for a finite element formulation that includes continuity of interlaminar shear stresses.

3.1. Virtual work equation. Stress resultants

Equilibrium of the composite shell may be enforced through the principle of virtual work: $G_{\text{int}}(\mathbf{U}; \delta\mathbf{U}) - G_{\text{ext}}(\delta\mathbf{U}) = 0$, where $G_{\text{int}}(\mathbf{U}; \delta\mathbf{U})$ is the internal part of the virtual work, while $G_{\text{ext}}(\delta\mathbf{U})$ is the part due to the virtual work of external forces. Internal part of the virtual work for the present composite shell model reads as

$$G_{\text{int}}(\mathbf{U}; \delta\mathbf{U}) = \int_S \int_{h-}^{h+} \sigma^{\alpha\beta} [\delta\varepsilon_{\alpha\beta} + \xi\delta\kappa_{\alpha\beta} + f(\xi)\delta\kappa_{\alpha\beta}^f] \mu \, d\xi \, dS$$

$$+ \int_S \int_{h-}^{h+} \sigma^{\alpha3} [\delta\gamma_{\alpha3} + f' \delta\gamma_{\alpha3}^f] \mu \, d\xi \, dS \tag{28}$$

where variations of strains are defined in (19), (21) and $dS = \|\mathbf{X}^0_{,1} \times \mathbf{X}^0_{,2}\| d\xi^1 d\xi^2$ is an area element of the middle surface. Equation (28) motivates definition of the following stress resultants:

$$N^{\alpha\beta} = \int_{h-}^{h+} \sigma^{\alpha\beta} \mu \, d\xi, \quad M^{\alpha\beta} = \int_{h-}^{h+} \sigma^{\alpha\beta} \xi \mu \, d\xi, \quad Q^{\alpha 3} = \int_{h-}^{h+} \sigma^{\alpha 3} \mu \, d\xi$$

$$\widetilde{M}^{\alpha\beta} = \int_{h-}^{h+} \sigma^{\alpha\beta} f(\xi) \mu \, d\xi, \quad \widetilde{Q}^{\alpha 3} = \int_{h-}^{h+} \sigma^{\alpha 3} f' \mu \, d\xi \tag{29}$$

where $\int_{h-}^{h+} (\circ) \, d\xi = \sum_{K=1}^{N_{\text{lay}}} \int_{h_K^-}^{h_K^+} (\circ) \, d\xi_K$. Stresses $\sigma^{\alpha\beta}$ and $\sigma^{\alpha 3}$ are obtained layer-wise through constitutive relations (26). Let us assume that the shell is loaded only on the top surface, S^+, and on the bottom surface, S^-, by pressure loadings $\mathbf{p}^+$ and $\mathbf{p}^-$, respectively. External part of the virtual work may be then written as

$$G_{\text{ext}}(\delta \mathbf{U}) = \int_{S^+} \mathbf{p}^+ \cdot \delta \mathbf{u} \, dS^+ + \int_{S^-} \mathbf{p}^- \cdot \delta \mathbf{u} \, dS^- \tag{30}$$

where $dS^+ = \mu^+ \, dS$, $dS^- = \mu^- \, dS$ and $\mu^+ = \mu|_{h+}$, $\mu^- = \mu|_{h-}$. Using (b) in the above expression gives

$$\begin{aligned} G_{\text{ext}}(\delta \mathbf{U}) = &\int_S (\mathbf{p}^+ \mu^+ + \mathbf{p}^- \mu^-) \delta \mathbf{u}^0 \, dS \\ &+ \int_S \left(\mathbf{p}^+ \frac{h}{2} \mu^+ - \mathbf{p}^- \frac{h}{2} \mu^- \right) \delta \mathbf{w} \, dS \\ &+ \int_S (\mathbf{p}^+ (-1)^{N_{\text{lay}}} \mu^+ + \mathbf{p}^- \mu^-) \delta \mathbf{D} \, dS \end{aligned} \tag{31}$$

Equation (31) motivates definition of the following external forces and couples:

$$\mathbf{F} = \mathbf{p}^+ \mu^+ + \mathbf{p}^- \mu^-, \quad \mathbf{M} = \mathbf{p}^+ \frac{h}{2} \mu^+ - \mathbf{p}^- \frac{h}{2} \mu^-, \quad \mathbf{W} = \mathbf{p}^+ (-1)^{N_{\text{lay}}} \mu^+ + \mathbf{p}^- \mu^- \tag{32}$$

It can be seen from (31) that forces related to the wrinkling of shell cross-sections appear in the external part of the virtual work. Note, that the second and third integrals in (31) become zero if the pressures act in the direction of middle surface normal. Extension of the above procedure to include body forces and concentrate forces and couples is straightforward.

3.2. Mixed variational formulation

The starting point for the displacement-based shell finite element approximation is the two-dimensional form of virtual work equation. However, in order to develop a finite element with interlaminar continuous shear stresses, we use mixed variational formulation, presented below in this section. The stationary point of the Reissner's variation theorem (as used for the present problem)

may be stated as

$$\delta I(\mathbf{U}, \sigma_K; \delta\mathbf{U}, \delta\sigma_K) = \int_S N^{\alpha\beta} \delta\varepsilon_{\alpha\beta}\,\mathrm{d}S + \int_S M^{\alpha\beta} \delta\kappa_{\alpha\beta}\,\mathrm{d}S + \int_S \widetilde{M}^{\alpha\beta} \delta\kappa^f_{\alpha\beta}\,\mathrm{d}S$$

$$+ \int_S (\delta\gamma)^{\mathrm{T}} \left(\sum_{K=1}^{N_{\mathrm{lay}}} \int_{h_K^-}^{h_K^+} \sigma_K \mu\,\mathrm{d}\xi_K \right) \mathrm{d}S$$

$$+ \int_S (\delta\gamma^f)^{\mathrm{T}} \left(\sum_{K=1}^{N_{\mathrm{lay}}} \int_{h_K^-}^{h_K^+} \sigma_K f_K' \mu\,\mathrm{d}\xi_K \right) \mathrm{d}S$$

$$+ \int_S \left[\sum_{K=1}^{N_{\mathrm{lay}}} \int_{h_K^-}^{h_K^+} (\delta\sigma_K)^{\mathrm{T}}(-[\mathbf{C}_K^s]^{-1}\sigma_K + \gamma + f_K'\gamma^f)\mu\,\mathrm{d}\xi_K \right] \mathrm{d}S$$

$$- \int_S (\mathbf{F}\cdot\delta\mathbf{u}^0 + \mathbf{M}\cdot\delta\mathbf{w} + \mathbf{W}\cdot\delta\mathbf{D})\,\mathrm{d}S = 0 \tag{33}$$

where σ_K is a vector of assumed transverse shear stresses defined in (12), γ and γ^f are vectors of transverse shear strains (see (16) and (18))

$$\gamma = [\gamma_{13}, \gamma_{23}]^{\mathrm{T}}, \quad \gamma^f = [\gamma^f_{13}, \gamma^f_{23}]^{\mathrm{T}} \tag{34}$$

$[\mathbf{C}_K^s]^{-1}$ is an inverse of constitutive matrix $(27)_2$, stress resultants $N^{\alpha\beta}$, $M^{\alpha\beta}$ and $\widetilde{M}^{\alpha\beta}$ are defined in (29), $\delta\gamma$, $\delta\gamma^f$ and $\delta\mathbf{U} = [\delta\mathbf{u}^0, \delta\mathbf{w}, \delta\mathbf{D}]^{\mathrm{T}}$ are variations of (34) and (7), respectively, while strain variations, $\delta\varepsilon_{\alpha\beta}$, $\delta\kappa_{\alpha\beta}$, $\delta\kappa^f_{\alpha\beta}$, are given in (19) and (21). Equation (33) is a base for the finite element formulation presented in Section 5. A procedure to express σ_K with $\mathbf{U}$, and thus transfer mixed formulation (33) to the displacement-like, is provided in detail in Section 4.

3.3. Constitutive relations

In this section we analytically integrate lamina constitutive relations (see Section 2.5) through the shell thickness to obtain relations between stress resultants and strains. Variation of metrics through the thickness is neglected, i.e. it is assumed that $\mu = 1$. In accordance with (29) and (18), we introduce the following two vectors of stress resultants and strains:

$$\mathbf{N} = [N^{11}, N^{22}, N^{12}; M^{11}, M^{22}, M^{12}; Q^{13}, Q^{23}; \widetilde{M}^{11}, \widetilde{M}^{22}, \widetilde{M}^{12}; \widetilde{Q}^{13}, \widetilde{Q}^{23}]^{\mathrm{T}}_{(13\times 1)}$$

$$\varepsilon = [\varepsilon_{11}, \varepsilon_{22}, \varepsilon_{12}; \kappa_{11}, \kappa_{22}, \kappa_{12}; \gamma_{13}, \gamma_{23}; \kappa^f_{11}, \kappa^f_{22}, \kappa^f_{12}; \gamma^f_{13}, \gamma^f_{23}]^{\mathrm{T}}_{(13\times 1)} \tag{35}$$

which are related through matrix H as

$$\mathbf{N} = \mathbf{H}\varepsilon \tag{36}$$

Using definition of stress resultants, (29), and layer constitutive relations, (26), we have

$$
H = \begin{bmatrix}
C_0 & C_1 & 0_{(3\times2)} & F_{10} & 0_{(3\times2)} \\
 & C_2 & 0_{(3\times2)} & F_{11} & 0_{(3\times2)} \\
 & & Z_0 & 0_{(2\times3)} & Z_1 \\
 & & & F_{02} & 0_{(3\times2)} \\
\text{symm.} & & & & Z_2
\end{bmatrix}_{(13\times13)}
\tag{37}
$$

where sub-matrices of H are defined as

$$
C_J = \sum_{K=1}^{N_{lay}} \int_{h_K^-}^{h_K^+} C_K \xi^J \mu \, d\xi_K, \quad Z_J = \sum_{K=1}^{N_{lay}} \int_{h_K^-}^{h_K^+} C_K^s [f_K']^J \mu \, d\xi_K
$$

$$
F_{IJ} = \sum_{K=1}^{N_{lay}} \int_{h_K^-}^{h_K^+} C_K \xi^I [f(\xi_K)]^J \mu \, d\xi_K, \quad J = 0,1,2, \; I = 0,1
\tag{38}
$$

C_J, Z_J and F_{IJ} are (3×3), (2×2) and (3×3) matrices, respectively, while C_K and C_K^s are given in (27). The following constants may be obtained by an integration of expressions (38)

$$
(C_0, C_1, C_2) \overset{\mu=1}{=} \sum_{K=1}^{N_{lay}} \left(h_K, \frac{(h_K^+)^2 - (h_K^-)^2}{2}, \frac{(h_K^+)^3 - (h_K^-)^3}{3} \right) C_K
$$

$$
(Z_0, Z_1, Z_2) \overset{\mu=1}{=} \sum_{K=1}^{N_{lay}} \left(h_K, 2(-1)^K, \frac{4}{h_K} \right) C_K^s
\tag{39}
$$

$$
(F_{10}, F_{11}, F_{02}) \overset{\mu=1}{=} \sum_{K=1}^{N_{lay}} \left(0, \frac{(-1)^K h_K^2}{6}, \frac{h_K}{3} \right) C_K
$$

It must be noted, that the coefficients of H, given in (39), are valid only for the pure displacement formulation. Since we work with mixed formulation (33), the Z_J matrices change to

$$
(Z_0, Z_1, Z_2) \overset{\mu=1}{=} \sum_{K=1}^{N_{lay}} (Q_K^0, Q_K^1, f_K' Q_K^1)
\tag{40}
$$

where Q_K^0 and Q_K^1 are provided in Section 4 and in Appendix A.

4. ELIMINATION OF STRESS VARIABLES

The model based on mixed principle (33) has: (i) 7 displacement unknowns (see (7)) and (ii) $6 \times N_{lay}$ stress unknowns (see (11)$_1$). In order to preserve the advantages of displacement-like formulation, the stress unknowns should be expressed in terms of the displacement ones. For plates, such a procedure was developed by Carrera (see References [4, 24]), who recently reformulated

it in Reference [29] to make it more transparent for the finite element implementation. This reformulated procedure is in this section (and in Appendix A) extended to shells.

4.1. Layer stress–displacement relations

By observing (33), it can be seen that we have to satisfy the following functional for each layer $K \in [1, N_{\text{lay}}]$:

$$F(\mathbf{U}; \delta\sigma_K) = \int_{h_K^-}^{h_K^+} (\delta\sigma_K)^{\mathrm{T}} [\gamma(\mathbf{U}) + f_K' \gamma^f(\mathbf{U}) - \mathbf{S}_K \sigma_K] \mu \, \mathrm{d}\xi_K = 0 \tag{41}$$

where vector σ_K is given in $(11)_2$, $\mathbf{S}_K$ is the compliance matrix

$$\mathbf{S}_K = [\mathbf{C}_K^s]^{-1} = \begin{bmatrix} \mathbf{S}_{44} & \mathbf{S}_{45} \\ \text{symm.} & \mathbf{S}_{55} \end{bmatrix} = \begin{bmatrix} \mathbf{C}_K^{1313} & \mathbf{C}_K^{1323} \\ \text{symm.} & \mathbf{C}_K^{2323} \end{bmatrix}^{-1} \tag{42}$$

while strain–displacement operators γ and γ^f may be written as, see (18),

$$\gamma + f_K' \gamma^f = \left\{ \begin{array}{c} \gamma_{13} + f_K' \gamma_{13}^f \\ \gamma_{23} + f_K' \gamma_{23}^f \end{array} \right\} = [\mathbf{b}_0 + f_K' \mathbf{b}_1] \mathbf{U} \tag{43}$$

where $\mathbf{U}$ is given in (7), while $\mathbf{b}_0$ and $\mathbf{b}_1$ are

$$\mathbf{b}_0 = \begin{bmatrix} \mathbf{0}_{(1\times3)} & (\mathbf{X}_{,1}^0)^{\mathrm{T}}\mathbf{A} & \mathbf{0}_{(1\times2)} \\ \mathbf{0}_{(1\times3)} & (\mathbf{X}_{,2}^0)^{\mathrm{T}}\mathbf{A} & \mathbf{0}_{(1\times2)} \end{bmatrix}_{(2\times7)}, \quad \mathbf{b}_1 = \begin{bmatrix} \mathbf{0}_{(1\times3)} & \mathbf{0}_{(1\times2)} & (\mathbf{X}_{,1}^0)^{\mathrm{T}}\tilde{\mathbf{Q}} \\ \mathbf{0}_{(1\times3)} & \mathbf{0}_{(1\times2)} & (\mathbf{X}_{,2}^0)^{\mathrm{T}}\tilde{\mathbf{Q}} \end{bmatrix}_{(2\times7)} \tag{44}$$

$\mathbf{A}$ and $\tilde{\mathbf{Q}}$ are defined in (20) and $(6)_2$. By using (12) and (43), we may rewrite (41) as

$$\int_{h_K^-}^{h_K^+} (\delta\chi_K)^{\mathrm{T}} \{[\mathbf{E}^{\mathrm{T}}(\mathbf{b}_0 + f_K' \mathbf{b}_1)]\mathbf{U} - \mathbf{E}^{\mathrm{T}}\mathbf{S}_K \mathbf{E}\chi_K\} \mu \, \mathrm{d}\xi_K = 0 \tag{45}$$

Expression (45) motivates definition of the following two matrices:

$$\mathbf{H}_K^u = \left(\int_{h_K^-}^{h_K^+} \mathbf{E}^{\mathrm{T}} \mu \, \mathrm{d}\xi_K \right) [\mathbf{b}_0 + f_K' \mathbf{b}_1] = \begin{bmatrix} \mathbf{0}_{(2\times7)} \\ \mathbf{b}_0 + f_K' \mathbf{b}_1 \\ \mathbf{0}_{(2\times7)} \end{bmatrix}_{(6\times7)} \tag{46}$$

and

$$\mathbf{H}_K^\sigma = \int_{h_K^-}^{h_K^+} \mathbf{E}^T \mathbf{S}_K \mathbf{E} \mu \, d\xi_K$$

$$= \begin{bmatrix}
\dfrac{2S_{44}h_K}{15} & \dfrac{2S_{45}h_K}{15} & -\dfrac{S_{44}}{10} & -\dfrac{S_{45}}{10} & -\dfrac{S_{44}h_K}{30} & -\dfrac{S_{45}h_K}{30} \\[2mm]
 & \dfrac{2S_{55}h_K}{15} & -\dfrac{S_{45}}{10} & -\dfrac{S_{55}}{10} & -\dfrac{S_{45}h_K}{30} & -\dfrac{S_{55}h_K}{30} \\[2mm]
 & & \dfrac{6S_{44}}{5h_K} & \dfrac{6S_{45}}{5h_K} & -\dfrac{S_{44}}{10} & -\dfrac{S_{45}}{10} \\[2mm]
 & & & \dfrac{6S_{55}}{5h_k} & -\dfrac{S_{45}}{10} & -\dfrac{S_{55}}{10} \\[2mm]
 & & & & \dfrac{2S_{44}h_K}{15} & \dfrac{2S_{45}h_K}{15} \\[2mm]
\text{symm.} & & & & & \dfrac{2S_{55}h_K}{15}
\end{bmatrix}_{(6\times6)} \tag{47}$$

Note, that (15) was used to obtain the final form of $\mathbf{H}_K^u$ in (46). Finally, by using (45)–(47), the functional (41) may be rewritten as

$$(\delta\boldsymbol{\chi}_K)^T[\mathbf{H}_K^u\mathbf{U} - \mathbf{H}_K^\sigma\boldsymbol{\chi}_K] = 0 \tag{48}$$

From (48) it is possible to express layer stress parameters as functions of $\mathbf{U}$.

4.2. Interlaminar shear stress continuity

We now use (48) for each layer $K \in [1, N_{lay}]$ to obtain the following relation for the cross-section of multilayered shell:

$$\{\delta\chi_{N_{lay}}, \delta\chi_{N_{lay}-1}, \ldots, \delta\chi_1\}^T \left(\widetilde{\mathbf{H}}^u\mathbf{U} - (\widetilde{\mathbf{H}}^\sigma) \begin{Bmatrix} \chi_{N_{lay}} \\ \chi_{N_{lay}-1} \\ \vdots \\ \chi_1 \end{Bmatrix} \right) = 0 \tag{49}$$

where $\widetilde{\mathbf{H}}^\sigma$ is a block diagonal matrix composed of matrices (47), i.e.

$$\widetilde{\mathbf{H}}^\sigma = \text{Diag}[\mathbf{H}_{N_{lay}}^\sigma, \mathbf{H}_{N_{lay}-1}^\sigma, \ldots, \mathbf{H}_1^\sigma]_{(6N_{lay} \times 6N_{lay})} \tag{50}$$

while $\widetilde{\mathbf{H}}^u$ is defined as a composition of matrices (46)

$$\widetilde{\mathbf{H}}^u = [\mathbf{H}_{N_{lay}}^u, \mathbf{H}_{N_{lay}-1}^u, \ldots, \mathbf{H}_1^u]_{(6N_{lay} \times 7)}^T \tag{51}$$

With (49), the stress unknowns at the multilayered (cross-section) level could be expressed. However, since there is no coupling between layers in (49), the result would be the same as when using (48) for each layer.

4.3. Cross-section stress–displacement relation

To enforce the continuity of the interlaminar shear stresses (i.e. the equilibrium conditions at layer interfaces) we have to satisfy the following conditions:

$$
\begin{aligned}
\sigma_{(K+1)}^{\alpha 3,\text{bot}} &= \sigma_K^{\alpha 3,\text{top}} && \text{if } K \in [1, N_{\text{lay}} - 1] \\
\sigma_K^{\alpha 3,\text{bot}} &= \overline{\sigma}^{\alpha 3,\text{bot}} && \text{if } K = 1 \\
\sigma_K^{\alpha 3,\text{top}} &= \overline{\sigma}^{\alpha 3,\text{top}} && \text{if } K = N_{\text{lay}}
\end{aligned}
\tag{52}
$$

where $\overline{\sigma}^{\alpha 3,\text{bot}}$ and $\overline{\sigma}^{\alpha 3,\text{top}}$ are applied stresses at the bottom and top surfaces of the shell, respectively. In this work we assume, without loss of generality, that $\overline{\sigma}^{\alpha 3,\text{bot}} = \overline{\sigma}^{\alpha 3,\text{top}} = 0$. To take into account (52), Equation (49) need to be modified (coupling between layers comes into the formulation). This modification is provided in detail in Appendix A.

Modified layer constitutive matrices may be obtained by the direct usage of (52) and (49) as shown in Reference [24] for plates. However, it proved more convenient to find layer-dependent matrices Q_K^0 and Q_K^1, defined as

$$
\int_{h_K^-}^{h_K^+} \sigma_K \mu \, \mathrm{d}\xi = (Q_K^0 \mathbf{b}_0 + Q_K^1 \mathbf{b}_1)\mathbf{U} = Q_K^0 \gamma + Q_K^1 \gamma^f
\tag{53}
$$

Those two matrices are obtained by manipulation of (49). Details are provided in Appendix A.

Since we use Q_K^0 and Q_K^1 in (40) and in constitutive matrix H (instead of $(39)_2$, $(38)_2$ and $(26)_2$), we may regard Equations (49) and (53) as the weak form of Hooke's law. Those two equations enable treatment of mixed functional (33) in the manner of displacement like.

5. FINITE ELEMENT APPROXIMATION

In this section the finite element implementation of the above-described multilayered shell model is briefly presented. An isoparametric four-noded element with local Cartesian co-ordinate systems, introduced at middle surface integration points (see also Reference [30]), is used.

5.1. Interpolation of geometry and physical fields

The geometry of the shell and the displacement variables are interpolated with standard bi-linear functions[‡] $N^I(\xi^1, \xi^2) = \frac{1}{4}(1 + \xi^1 \xi_I^1)(1 + \xi^2 \xi_I^2)$, where: $(\xi_I^1 = -1, +1, +1, -1)$, $(\xi_I^2 = -1, -1, +1, +1)$ for I given in the following order $(I = 1, 2, 3, 4)$; and $\xi^1 \in [-1, 1]$, $\xi^2 \in [-1, 1]$. Finite element approximation of the shell geometry over the finite element is given as

$$
\mathbf{X}^0 = \sum_{I=1}^{4} N^I(\xi^1, \xi^2)\mathbf{X}_I^0, \quad \mathbf{T} = \sum_{I=1}^{4} N^I(\xi^1, \xi^2)\mathbf{T}_I
\tag{54}
$$

where $\mathbf{X}_I^0$ defines the position of nodal middle surface point and $\mathbf{T}_I$ is shell director at this point. Description of shell geometry requires a knowledge of the position of shell director at nodal points of the finite element mesh. In the present formulation the nodal shell director is

---

[‡]In this section and in Appendix B we will also use notation $\xi^1 \equiv \xi$ and $\xi^2 \equiv \eta$.

obtained by averaging the nodal normals of adjoining elements: first, the element nodal normal is evaluated as

$$\mathbf{T}_I^e = (\mathbf{X}_J^0 - \mathbf{X}_I^0) \times (\mathbf{X}_K^0 - \mathbf{X}_I^0) \tag{55}$$

where I, J and K are given in the following order $(I = 1, 2, 3, 4)$, $(J = 2, 3, 4, 1)$, $(K = 4, 1, 2, 3)$; next, the averaged nodal normal of unit length is determined as

$$\widetilde{\mathbf{T}}_I = \frac{1}{N_{Iel}} \sum_I^{N_{Iel}} \mathbf{T}_I^e, \quad \mathbf{T}_I = \frac{\widetilde{\mathbf{T}}_I}{\|\widetilde{\mathbf{T}}_I\|} \tag{56}$$

where N_{Iel} is the number of adjoining elements at node 'I'. By using this approach some unavoidable discretization errors are introduced for curved geometries, however it seems that there is no more convenient way to define shell directors of the finite element mesh for four-noded elements.

Displacements are interpolated over the element as

$$\mathbf{u}^0 = \sum_{I=1}^4 N^I(\xi^1, \xi^2)\mathbf{u}_I^0, \quad \mathbf{w} = \sum_{I=1}^4 N^I(\xi^1, \xi^2)\mathbf{w}_I, \quad \mathbf{D} = \sum_{I=1}^4 N^I(\xi^1, \xi^2)\mathbf{D}_I \tag{57}$$

where the reduction of unknowns is given by discrete version of (20)

$$\delta\mathbf{w}_I = \mathbf{\Lambda}_I \begin{Bmatrix} \delta\alpha_I \\ \delta\beta_I \end{Bmatrix}, \quad \delta\mathbf{D}_I = \widetilde{\mathbf{Q}}_I \begin{Bmatrix} \delta(\widetilde{D}_1)_I \\ (\delta\widetilde{D}_2)_I \end{Bmatrix} \tag{58}$$

Transverse shear field is interpolated over the element by the so-called assumed natural strain (ANS) procedure [31]

$$\begin{aligned}
(\gamma_{13}, \gamma_{13}^f) &= \tfrac{1}{2}[1 - \xi^2](\gamma_{13}^A, \gamma_{13}^{f,A}) + \tfrac{1}{2}[1 + \xi^2](\gamma_{13}^C, \gamma_{13}^{f,C}) \\
(\gamma_{23}, \gamma_{23}^f) &= \tfrac{1}{2}[1 - \xi^1](\gamma_{23}^D, \gamma_{23}^{f,D}) + \tfrac{1}{2}[1 + \xi^1](\gamma_{23}^B, \gamma_{23}^{f,B})
\end{aligned} \tag{59}$$

Accordingly, the transverse shear stresses $\gamma_{\alpha3}$ and $\gamma_{\alpha3}^f$ are evaluated using kinematic relations only at points A, B, C and D. However, since strains at those points are functions of nodal displacements, the explicit evaluation of transverse shear strains at points A, B, C and E may be avoided in the computational process.

5.2. Local co-ordinate systems

Two types of local Cartesian co-ordinate systems are needed in the present finite element approximation: (i) local co-ordinate systems at nodes of the finite element mesh and (ii) local co-ordinate systems at finite element integration points. Both types are determined by an analogous procedure. Base vectors associated to the nodal co-ordinate system at the mesh point 'I' are defined with the following relations:

$$(\mathbf{E}_3)_I = \mathbf{T}_I, \quad (\mathbf{E}_1)_I \times (\mathbf{E}_2)_I = \mathbf{T}_I, \quad (\mathbf{E}_1)_I \cdot (\mathbf{E}_2)_I = 0 \tag{60}$$

Note, that positions of vectors $(\mathbf{E}_1)_I$ and $(\mathbf{E}_2)_I$ are arbitrary, as long as they satisfy conditions (60). Base vectors $\{\mathbf{E}_i\}$ related to the co-ordinate system $(\hat{x}, \hat{y}, \hat{z})$ at element integration point are defined analogously to (60) (see also Section 2.2). The introduced change of co-ordinates at

element integration points requires transformation for partial differentiation. It can be shown that the shape function derivatives with respect to the local Cartesian co-ordinates can be obtained as

$$\begin{Bmatrix} N^I_{,\hat{x}} \\ N^I_{,\hat{y}} \end{Bmatrix} = \begin{bmatrix} \dfrac{\partial \xi}{\partial \hat{x}} & \dfrac{\partial \eta}{\partial \hat{x}} \\ \dfrac{\partial \xi}{\partial \hat{y}} & \dfrac{\partial \eta}{\partial \hat{y}} \end{bmatrix} = \begin{bmatrix} \mathbf{E}_1 \cdot \mathbf{X}^0_{,\xi} & \mathbf{E}_2 \cdot \mathbf{X}^0_{,\xi} \\ \mathbf{E}_1 \cdot \mathbf{X}^0_{,\eta} & \mathbf{E}_2 \cdot \mathbf{X}^0_{,\eta} \end{bmatrix}^{-1} \begin{Bmatrix} N^I_{,\xi} \\ N^I_{,\eta} \end{Bmatrix} \tag{61}$$

5.3. Discrete form of mixed variational equation

By inserting the above interpolations, the results of derivations of Section 4 (and Appendix A) and Equation (36) into the mixed functional (33), we get the following (displacement-like) discrete version of (33):

$$\bigcup_{e=1}^{N_{\text{elem}}} \int_{S_e} (\delta \varepsilon)^{\mathrm{T}} \mathsf{H} \varepsilon \, \mathrm{d}S_e - \bigcup_{e=1}^{N_{\text{elem}}} \int_{S_e} (\delta \mathbf{U})^{\mathrm{T}} \mathbf{P} \, \mathrm{d}S_e = 0 \tag{62}$$

where vector ε and matrix H are given in (35) and (37), respectively, $\delta\varepsilon$ is variation of ε, and $\mathbf{P}$ represents a vector of external forces $\mathbf{P} = [\mathbf{F}, \mathbf{M}, \mathbf{W}]^{\mathrm{T}}$, see (32). Note, that Z_0, Z_1 and Z_2 sub-matrices of H are defined by (40). Q^0_K and Q^1_K matrices of (40) are provided in (77). Explicit expressions for $\delta\varepsilon$ and ε are given in Appendix B.

6. NUMERICAL EXAMPLES

In this section three numerical examples are presented in order to illustrate the performance capabilities of the described refined multilayered shell model and associated finite element formulation based on the four-noded element. A compendium of acronyms, used to denote models chosen for comparison with the present model, is given in Table I; the proposed formulation is denoted by the acronym RMZC.

All the examples below relate to three-layered, cross ply laminated shells. The subscripts 1 and 2 are used to denote the direction of two orthogonal co-ordinates lying on the tangent plane to the reference (middle) surface of the shell, while the subscript 3 denotes the co-ordinate in the thickness direction. Since the finite element formulation is based on the four-noded element with linear interpolation functions, the transverse shear stresses cannot be evaluated a posteriori via an integration of three-dimensional equilibrium equations. Such an evaluation would require the use of eight- or nine-noded elements. All the transverse shear stresses shown in this paper are therefore obtained a priori, directly from the assumed shear stress model. Geometry for all three examples is shown in Figure 3.

Example 6.1. Square and rectangular plate loaded by bi-sinusoidal transverse pressure.

Exact solution of this standard benchmark test was given by Pagano and Hatfield [32]. First we consider a simply supported, three-layered, [0°/90°/0°] square plate with length a, loaded by

Table I. List of acronyms used to denote models; in alphabetic order.

Exact	Three-dimensional solutions
CLT	Classical lamination theory
D&R	Hybrid FE [19]
EM3(2, 1)	ESLM mixed [35]
EM3(2, 1)*	ESLM mixed [35], discarding σ_{zz}
FSDT	First-order shear deformation theory
F-J&T	FSDT by Jing and Tzeng [38]
F-K&K	FSDT by Kant and Khare [37]
L&S	Hybrid layer-wise FE [39]
HSDT	Higher-order shear deformation theory
H-B&V	HSDT by Bhaskar and Varadan [26]
H.a-B&V	H-B&V with shear stresses computed by assumed models
H.b-B&V	H-B&V with shear stresses computed via an integration of 3D equilibrium equations
H-D&P	HSDT by Dennis and Palazotto [36]
H-J&T	HSDT by Jing and Tzeng [38]
H-K&K	HSDT by Kant and Khare [37]
LM4(3, 2, 1)	Layer-wise mixed [8]
LD4(3, 2, 1)	Layer-wise for displacement [8]
RMZC	Present model, full implementation
Reddy-HSDT	HSDT by Reddy [40]
RMZ	Present model without interlaminar shear stress continuity
RMC	Present model without zig-zag effects as in Reference [41]
RM	Present FSDT case
RMs	Present RM case with shear correction factor $\chi = \frac{5}{6}$
RMp	Present CLT analysis
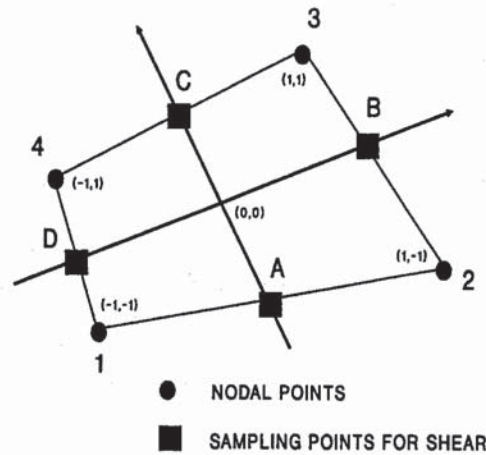
Figure 3. Four-noded shell finite element with assumed transverse shear strain fields.

bi-sinusoidal pressure $\bar{q} = q \sin(\pi x/a) \sin(\pi y/a)$ (origin of co-ordinates x and y is shown in Figure 3). The plate thickness is h, while the material characteristics are

$$E_{\mathrm{L}}/E_{\mathrm{T}} = 25, \quad G_{\mathrm{LT}}/E_{\mathrm{T}} = 0.5, \quad G_{\mathrm{TT}}/E_{\mathrm{T}} = 0.2, \quad \nu_{\mathrm{LT}} = 0.25 \tag{63}$$

where, following usual notations, L is a direction of the fibres, T is the transverse direction and ν_{LT} is the major Poisson's ratio. The thickness of 0° layers is $h/4$ and the thickness of 90° layer is $h/2$. Following [32], the non-dimensional displacements and stresses

$$\bar{u}_3 = u_3 \frac{100 E_T h^3}{qa^4}, \quad (\bar{\sigma}_{11}, \bar{\sigma}_{12}) = (\sigma_{11}, \sigma_{12}) \frac{h^2}{qa^2} \tag{64}$$

are introduced for the presentation of results.

One-quarter of the plate is discretized by 16×16 finite elements, restricting deformations to be symmetric along the lines of the symmetry. Results are shown in Table II(a): the non-dimensional transversal displacement $\bar{u}_3$ at $(a/2, a/2, 0)$ and non-dimensional stresses $\bar{\sigma}_{11}, \bar{\sigma}_{12}$ at the closest integration point to $(a/2, a/2)$ and $(0, 0)$, respectively. The values are compared with the exact solution and with the HSDT of Pandya and Kant [33] (which preserves the C^0-continuity of displacements but does not include the zig-zag effects, neither fulfills the interlaminar continuity). Some differences between the results obtained by the present formulation and the results presented by RMZC plate formulation [24] (see Table 6 in Reference [24]) may be due to the different ways of elimination of shear locking effect (ANS concept in this work, selective integration in Reference [24]) as well as to the different meshes used. It can be seen from Table II(a), that the RMZC model considerably improves the FSDT analysis (RMs in Table II(a)). The CLT results (RMp in Table II(a)) are obtained by the simple penalty technique. It may be noted, that the use of shear correction factor in FSDT analysis (RMs) leads to results with thickness-dependent accuracy (see e.g. discussion of Noor and Peters [34]). It should be also noted, that the neglection of σ_{33} stresses makes the two-dimensional models unable to predict the unsymmetrical stress distribution in the case of very thick plates.

A more comprehensive comparison of different laminated theories is provided in Table IIb. Finite element and analytical closed-form solutions are compared to the exact solution for a rectangular plate. Results of LWM and ESLM proposed by Carrera in References [8, 35] are also shown: LM denotes mixed models with linear to the fourth-order variation of displacements and stresses in each layer (suffix 1, 2, 3, 4, respectively); LD denotes the correspondent displacement formulation; EM denotes the models that are an extension of the RMZC models (EM models discard σ_{zz}) since they use higher-order polynomials for both displacements and transverse stresses. It can be seen from Table IIb, that the layer-wise mixed analysis leads to the best results. RMZC results are very close to those obtained by Di and Ramm [19], who used hybrid formulations. Note, that the transverse normal stress does not play an important role in this example. As shown in Reference [35], this role increases by increasing thickness and/or transverse anisotropy. EM-3 case shows that the extension of RMZC to higher-order diplacement field would lead to better results. On the other hand, such an extension would introduce additional degrees of freedom and an increase of computational costs. The small differences between RMZC and EM-1* results may be addressed to the finite element approximation.

Example 6.2. Shell panel subjected to cylindrical bending.

Exact solution for the problem of simply supported cylindrical panel of infinite length, which is loaded by sinusoidally distributed pressure, was given by Ren [2] (Figure 4). Geometric characteristics of three-layered [90°/0°/90°] panel are: $R/b = 3/\pi$, where R is its radius and b is its arc-length in the circumferential direction; h is the thickness of the shell and $h/3$ is the thickness of each layer. Material characteristics are the same as those for plates, see (63). For 90° layer

fibres are parallel to the circumferential co-ordinate b. Sinusoidally distributed transverse pressure $\bar{q} = q \sin(3\varphi) = q \sin(\pi a/b)$, where $\varphi \in [0, \pi/3]$ and $a \in [0, b]$, is applied on the top surface. Non-dimensional displacements and stresses are for this case defined as

$$\bar{u}_3 = u_3 \frac{10\,E_T\,h^3}{qR^4}, \quad \bar{u}_2 = u_2 \frac{100\,E_T\,h^2}{qR^3}, \quad \bar{\sigma}_{22} = \sigma_{22} \frac{h^2}{qR^2}, \quad \bar{\sigma}_{23} = \sigma_{23} \frac{h}{qR} \tag{65}$$

Due to the symmetry, one-half of the panel in the circumferential direction was discretized, taking into account the symmetry conditions. The panel's length is infinite, therefore a unit length may be taken for the analysis. Only one element is used for discretization in that direction, while different number of elements are used for discretization in the circumferential direction. Variations of stresses $\bar{\sigma}_{22}, \bar{\sigma}_{23}$ and displacements $\bar{u}_2, \bar{u}_3$ with respect to the number of used finite elements (for one-half of the panel) are shown in Table III and Figure 5. Values are normalized with those obtained by 48 × 1 mesh. (Exact values for $\bar{u}_3$, $\bar{\sigma}_{22t}$ and $\bar{\sigma}_{22b}$ are 0.0787, 0.781 and -0.786, respectively). The transverse displacement $\bar{u}_3$ and in-plane circumferential stress $\bar{\sigma}_{22}$ are taken from the centre of the panel, i.e. at $a = b/2$ or at a closest integration point. The circumferential displacement $\bar{u}_2$ and transverse shear $\bar{\sigma}_{23}$ are taken at $a = 0$ or at a closest integration point. Value of $\bar{\sigma}_{23}$ in Table III is at the middle surface, i.e. at $\xi = 0$. Transverse shear stress $\bar{\sigma}_{23}$ is evaluated at the middle surface. In Figure 5 the subscripts t and b denote values at the top and bottom surfaces of the panel, respectively. It can be seen from Figure 5 and Table III that all the values increase monotonically with the number of elements and that the convergence for displacements is slightly different from the convergence of stresses.

Table II(a). Square plate: Present versus exact solutions. Mesh is 16 × 16 finite elements for one quarter of a plate.

a/h	2	4	10	100
			$\bar{u}_3$	
Exact	5.1964	1.9368	0.7370	0.4347
HSDT [33]	—	1.8744	0.7185	0.4346
RMZC	5.4081	1.9625	0.7373	0.4336
RMZ	5.1451	1.9034	0.7284	0.4335
RMs	5.0576	1.7073	0.6615	0.4327
RMp	0.4301	0.4302	0.4302	0.4302
			$\bar{\sigma}_{11}$	
Exact	1.3880	0.7299	0.5590	0.5390
	-0.0795			
HSDT [33]	—	0.7163	0.5676	0.5442
RMZC	0.8742	0.6430	0.5469	0.5365
RMZ	0.8875	0.6394	0.5459	0.5365
RMs	0.3380	0.4041	0.4970	0.5360
			$\bar{\sigma}_{12}$	
Exact	0.0863	0.0467	0.0275	0.0214
	-0.0673			
HSDT [33]	—	0.0454	0.0273	0.0215
RMZC	0.0711	0.0449	0.0273	0.0213
RMZ	0.0690	0.0442	0.0271	0.0213
RMs	0.0354	0.0307	0.0240	0.0212

Table II(b). Rectangular plate $b = 3a$: Present versus other FEM, analytical ESLM and analytical LWM solutions for $\bar{u}_3$.

a/h	4	10	20	100
Exact	2.8200	0.919	0.6100	0.5080
FEM solutions				
L&S	2.828	0.921	0.611	—
D&R	2.8370	0.920	0.6086	0.5061
RMZC	2.8371	0.914	0.6061	0.5048
Analytical closed-form solutions				
Layer-wise models				
LM4	2.8211	0.9189	0.6095	0.5077
LM3	2.8216	0.9189	0.6095	0.5077
LM2	2.8250	0.9120	0.6096	0.5077
LM1	2.7296	0.9097	0.6076	0.5076
LD4	2.8211	0.9189	0.6095	0.5077
LD3	2.8151	0.9189	0.6095	0.5077
LD2	2.7983	0.9181	0.6095	0.5077
LD1	2.7209	0.8988	0.6040	0.5071
Equivalent single-layer models				
EM3	2.8153	0.9181	0.6095	0.5077
EM2	2.7670	0.9055	0.6059	0.5075
EM1	2.8385	0.9150	0.6064	0.5051
EM3*	2.8325	0.9177	0.6073	0.5077
EM2*	2.7841	0.9042	0.6036	0.5075
EM1* = RMZC	2.8385	0.9150	0.6064	0.5051
Reddy-HSDT	2.6411	0.862	0.5937	0.5070
FSDT	2.0511	0.7504	0.5633	0.5033
CLT		0.503		

In Table IV, a comparison with the exact and other analytical and two-dimensional finite element solutions is made for $\bar{u}_3$ (for the mesh of 48×1 elements). Good performance of the present model found for the plate case may be also confirmed for this example of pure cylindrical bending. In particular, the results of the shell RMZC model are much closer to the exact ones than the results of HSDT model of Dennis and Palazooto [36] or Kant and Khare [37] (Figure 6). On the other hand, a superiority of layer-wise mixed models (M–p in Table IV) is shown for very thick shells (see also Reference [8]). As shown in Figure 7, the predicted distribution of in-plane displacements in the thickness directions is in good agreement with the analytical solution. The inefficiency of FSDT analysis is evident from this figure. In Figure 8, values of the transverse shear stress, evaluated *a priori* at layer interfaces, are compared to those obtained by Jing and Tzeng [38], who integrated the 3D indefinite equilibrium equations. It may be observed that the present evaluation of transverse stresses gives the same accuracy as that reported in Reference [38]. Exact as well as layer-wise mixed results are also quoted in Figure 8.

Example 6.3. Cylindrical shell subjected to internal pressure.

Exact solution for this example was given by Varadan and Bhaskar [3]. Basic geometrical characteristic of three-layered [90°/0°/90°] shell is $a/R = 4$, where a is the length of the cylinder
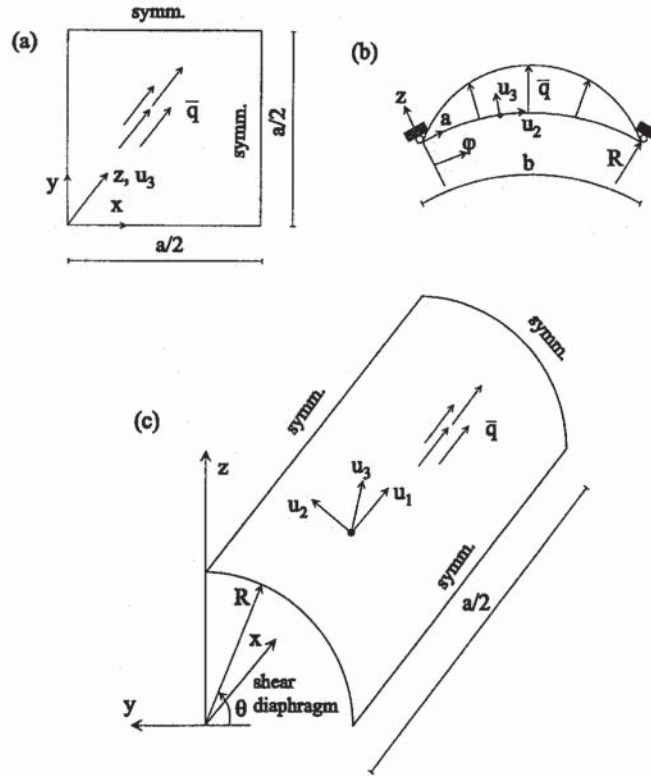
Figure 4. Geometry of examples: (a) plate; (b) shell panel; (c) cylindrical shell.

and R_2 is its radius. Thickness of the shell is denoted by h. Layer thickness of each layer is $h/3$. The cylinder is supported by shear diaphragms at both ends and it is subjected to transverse pressure, q, harmonically distributed on the shell internal surface as

$$\bar{q} = q \sin \frac{\pi x}{a} \cos 4\theta \tag{66}$$

where $x \in [0, a]$ and $\theta \in [0, 2\pi]$. Material characteristics are the same as those for a plate, see (63). For $0°$ layer fibres are parallel to the longitudinal co-ordinate x.

Due to the symmetry, only one-eighth of the cylinder (for $\theta \in [0, \pi/2]$ and $x \in [0, a/2]$) is discretized by finite elements, restricting deformations to be symmetric at the lines of the symmetry. Discretization in the longitudinal direction is done by 16 elements, while different number of elements are used for the circumferential discretization. Boundary conditions at the end ($u_1 \neq 0$, $u_2 = u_3 = 0$, where u_1 is longitudinal displacement, u_2 is circumferential displacement and u_3 is transverse displacement) are simulated by seven displacement degrees of freedom, i.e. by three global displacements, two rotations and two refined displacements. The results are presented for

Table III. Stresses and diplacement versus number of elements for $a/h = 100$.

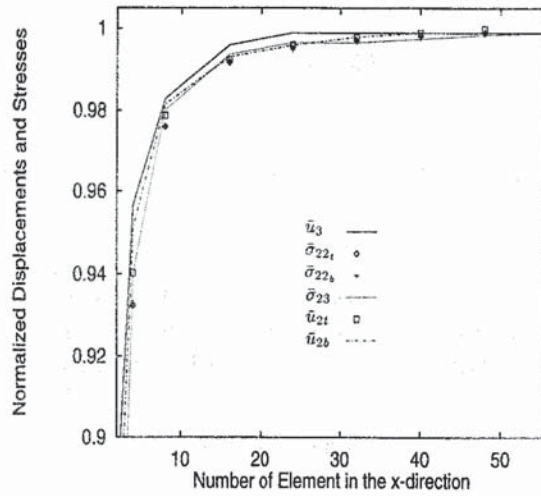| | Shell panel | | | | | |
	2×1	4×1	8×1	16×1	32×1	48×1
$\bar{u}_3$	0.0675	0.0759	0.0780	0.0785	0.0786	0.0787
$\bar{\sigma}_{22_t}$	0.6378	0.7425	0.7704	0.7775	0.7794	0.7797
$\bar{\sigma}_{22_b}$	-0.6428	-0.7479	-0.7831	-0.7831	-0.7850	-0.7853
$\bar{\sigma}_{23}$	0.4992	0.5459	0.5690	0.5726	0.5735	0.5737
$\bar{u}_{2t}$	20.54	24.00	24.90	25.13	25.19	25.20
$\bar{u}_{2b}$	22.44	26.04	26.97	27.21	27.27	27.28
	Cylindrical shell					
	4×16	8×16	16×16	24×16	32×16	48×16
$\bar{u}_3$	0.2443	0.4050	0.4540	0.4635	0.4668	0.4690
$\bar{u}_{1b}$	-1.028	-1.142	-1.516	-1.534	-1.541	-1.545
$\bar{u}_{1t}$	-0.8398	-1.003	-1.160	-1.170	-1.174	-1.177
$\bar{u}_{2b}$	-5.455	-10.44	-12.07	-12.39	-12.51	-12.59
$\bar{u}_{2t}$	-4.295	-8.853	-10.37	-10.67	-10.77	-10.85
$\bar{\sigma}_{11}$		0.0428	0.0436	0.0429	0.0424	0.0418
$\bar{\sigma}_{22}$		1.980	1.955	1.896	1.859	1.815
$\bar{\sigma}_{12}$		-0.0108	-0.0196	-0.0223	-0.0236	-0.0248
$\bar{\sigma}_{23}$	-1.839	-2.954	-3.300	-3.367	-3.391	-3.408

Figure 5. Shell panel with $R_2/h = 4$. Stresses and displacements versus number of elements for RMZC four-noded shell element. Values are normalized with respect to solutions obtained by 48×1 mesh.

the following non-dimensional quantities (Table V):

$$\bar{u}_3 = u_3 \frac{10\,E_L\,h^3}{qR^4}, \qquad (\bar{u}_1, \bar{u}_2) = (u_1,\,u_2)\frac{10\,E_L\,h^2}{qR^3}$$

$$(\bar{\sigma}_{11}, \bar{\sigma}_{22}, \bar{\sigma}_{12}) = (\sigma_{11}, \sigma_{22}, \sigma_{12})\frac{10\,h^2}{qR^2}, \qquad (\bar{\sigma}_{13}, \bar{\sigma}_{23}) = (\sigma_{13}, \sigma_{23})\frac{10\,h}{qR} \qquad (67)$$

Table IV. Shell panel: comparison of results for $\bar{u}_3$.

| R/h	2	4	10	50	100
Exact	1.436	0.457	0.144	0.0808	0.0787
Analytical					
LM2	1.436	0.4582	0.1440	0.0808	0.0787
H-J&T	—	0.459	0.142	0.0802	0.0780
F-J&T	—	0.342	0.120	0.0793	0.0780
CLT [2]	0.0799	0.0781	0.0777	0.0776	0.0776
FEM					
H-D&P	1.141	0.382	0.128	0.0796	0.0781
F-K&K	1.1179	0.3367	0.1180	0.0779	0.0767
H-K&K	1.1670	0.3790	0.1273	0.0782	0.0766
RMZC	1.5600	0.4656	0.1430	0.0809	0.0787
RMZ	1.4763	0.4492	0.1400	0.0808	0.0787
RMC	1.3175	0.3625	0.1226	0.0800	0.0784
RM	1.1988	0.3359	0.1187	0.0798	0.0784
RMs	1.4175	0.3852	0.1260	0.0802	0.0785
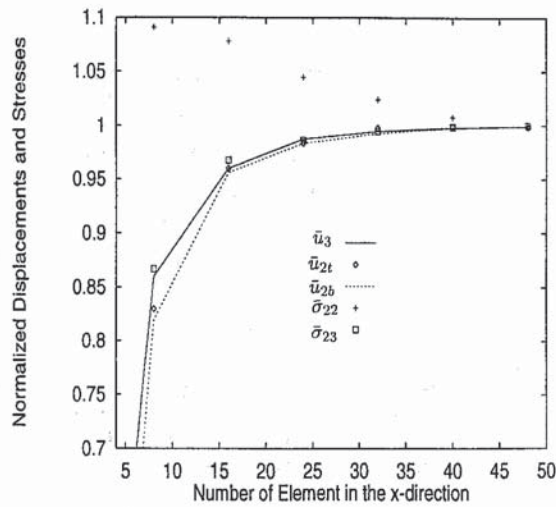
Figure 6. Cylindrical shell with $R_2/h = 4$. Stresses and displacements versus number of elements for RMZC four-noded shell element. Values are normalized with respect to solutions obtained by 48×16 mesh.

Variations of displacements and stresses with respect to the number of used finite elements are shown in Table III and in Figure 6. It can be seen that the convergence for stresses is better than for displacements, as expected. In Figure 6, the values are normalized with those obtained by 48×16 mesh. The subscripts t and b denote values at the top and at the bottom surface of the cylinder, respectively. Displacements u_1, u_2 and u_3 are taken at (x, θ) equal to $(0, 0)$, $(a/2, \pi/8)$ and $(a/2, \pi/2)$, respectively; stresses σ_{11}, σ_{22} and σ_{12} are taken at the closest integration point to $(a/4, \pi/16)$; and stresses σ_{23} are taken at the closest integration point to $(a/2, \pi/8)$. Comparison of
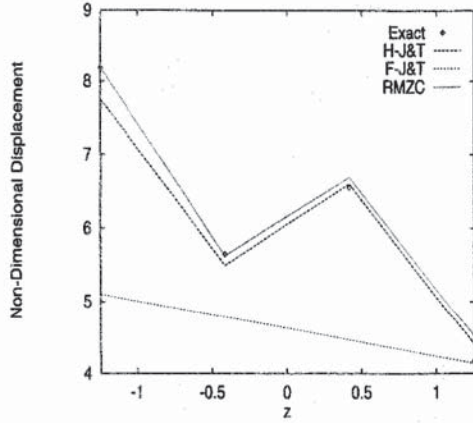
Figure 7. Shell panel with $R/h = 4$ ($h = 2.5$). Distribution of in-plane displacement $\bar{u}_2$ through the thickness ($z = \xi$).
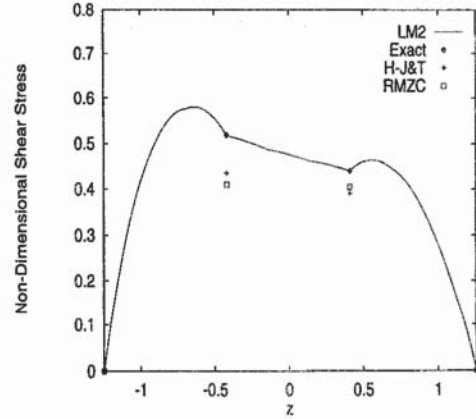

Figure 8. Shell panel with $R/h = 4$ ($h = 2.5$). Transverse shear stress $\bar{\sigma}_{23}$ ($z = \xi$).

Table V. Cylindrical shell: comparison of results for $\bar{u}_3$.

R/h	2	4	10	50	100
Exact	10.11	4.009	1.223	0.5495	0.4715
		Analytical			
H-B&V	—	3.923	1.210	—	—
HSDTA [42]	—	3.873	1.206	—	0.471
LM2	10.114	4.009	1.223	0.5495	0.4715
		FEM			
HSDT [42]	—	3.873	1.206	—	0.469
RMZC	10.996	4.003	1.207	0.5456	0.4683
RMZ	10.297	3.938	1.179	0.5444	0.4680
RMC	9.772	3.186	0.986	0.5362	0.4665
RM	8.878	2.926	0.941	0.5344	0.4660
RMs	10.541	3.409	1.025	0.5376	0.4668

RMZC results with the exact solution and some analytical and finite element results is made in Table VI. Values for σ_{11}, σ_{22} and σ_{12} in Tables III and VI are at the top surface of the shell (at $\xi = h/2$), while values for σ_{23} are at middle surface (at $\xi = 0$). Although there is a complex state of membrane and bending deformations is the cylinder, the results obtained by RMZC shell model are in good agreement with exact solutions and with results of representative HSDT model. In Figure 9, values of the transverse shear stress, evaluated *a priori* at layer interfaces, are compared to exact solution and to the results obtained by HSDT of Bhaskar and Varadan and by mixed model of Carrera.

Table VI. Cylindrical shell: comparison of results for stresses and displacements.

|	Exact	RMZC	HSDTa [30]	HDST [30]
		$a/h = 4$		
$\bar{u}_{1b}$	—	−1.8094	−1.753	−1.753
$\bar{u}_{1t}$	—	0.8239	0.806	0.806
$\bar{\sigma}_{11t}$	0.064	0.0596	0.061	0.064
$\bar{\sigma}_{22t}$	3.272	3.2207	3.339	3.272
$\bar{\sigma}_{12t}$	0.054	0.0450	0.046	0.054
		$a/h = 10$		
$\bar{u}_{1b}$	—	−0.8135	−0.808	−0.808
$\bar{u}_{1t}$	—	0.0968	0.103	0.102
$\bar{\sigma}_{11t}$	0.037	0.0362	0.036	0.037
$\bar{\sigma}_{22t}$	2.341	2.3738	2.361	2.347
$\bar{\sigma}_{12t}$	0.019	0.0154	0.017	0.019
		$a/h = 100$		
$\bar{u}_{1b}$	—	−1.5430	−1.541	−1.549
$\bar{u}_{1t}$	—	−1.1755	−1.172	−1.179
$\bar{\sigma}_{11t}$	0.042	0.0420	0.043	0.042
$\bar{\sigma}_{22t}$	1.753	1.8333	1.835	1.753
$\bar{\sigma}_{12t}$	−0.024	−0.0243	−0.024	−0.024
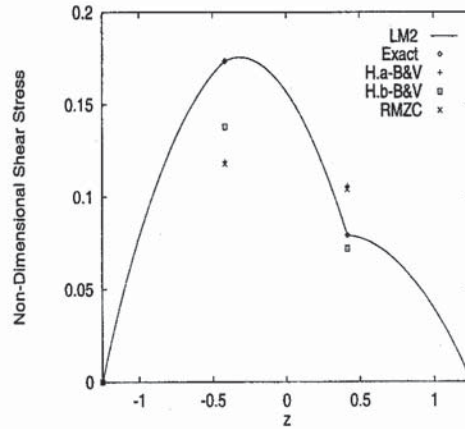
Figure 9. Cylindrical shell with $R/h = 4$ ($h = 2.5$). Transverse shear stress $\bar{\sigma}_{23}$ ($z = \xi$).

7. CONCLUSIONS

In this work a model for refined linear analysis of multilayered shells of moderate thickness is presented. The main features of the model can be briefly summarized as follows:

(i) To approximate displacement distribution across the thickness, the FSDT assumption of its linear through-thickness variation is refined by adding a zig-zag-shaped C^0 function and two additional displacements related to the wrinkling of the cross-section. The resulting shell element has *seven* degrees of freedom per node.

(ii) *Reissner's mixed variational principle* is applied to fulfill the trasnverse shear stress continuity at the interfaces between two adjacent layers. Transverse shear stresses are assumed to vary quadratically through each layer. The resulting layer-dependent stress parameters are eliminated by variationally consistent procedure. As a result, a weak form of constitutive relations (the so-called weak form of Hooke's law) is obtained.

(iii) In contrast with the available fully mixed finite element formulations, the proposed RMZC shell element does not require stress variables as nodal unknowns. Furthermore, when compared to hybrid formulations, RMZC elements do not require an elimination of stress variable at an element level.

Numerical examples show that the present approach leads to better solutions for displacements and stresses in comparison with other refined models which do not take into account continuity of interlaminar stresses. In particular, results for moderately thick shells are in very good agreement with exact 3D solutions and with hybrid FE formulations.

However, since the present model neglects transverse normal stress and related effects (as do the other refined shell models which do not relate the number of degrees of freedom to the number of layers), future work will be directed towards inclusion of complete 3D stress state. In this context, the use of higher order displacement fields becomes essential to analyse thick, unsymmetrically laminated shells.

APPENDIX A. AN EXAMPLE OF WEAK FORM OF HOOKE'S LAW

A.1. Modification of stress parameter vectors

Let us first modify vectors $(11)_1$ in accordance with the interlaminar equilibrium conditions (52). We get

$$\widehat{\chi}_K = \begin{cases} \{\sigma_K^{13,\text{top}}, \sigma_K^{23,\text{top}}, R_K^{13}, R_K^{23}\}^T & \text{if } K \in [1, N_{\text{lay}} - 1] \\ \{R_K^{13}, R_K^{23}\}^T & \text{if } K = N_{\text{lay}} \end{cases} \tag{A1}$$

Collection of all $\widehat{\chi}_K$ vectors gives

$$\{\widehat{\chi}_{N_{\text{lay}}}, \widehat{\chi}_{N_{\text{lay}}-1}, \ldots, \widehat{\chi}_1\}^T \tag{A2}$$

Now we modify Equation (49) in accordance with (A2). The result may be written as

$$\{\delta\widehat{\chi}_{N_{\text{lay}}}, \delta\widehat{\chi}_{N_{\text{lay}}-1}, \ldots, \delta\widehat{\chi}_1\}^T \left(\widehat{\mathbf{H}}^u \mathbf{U} - (\widehat{\mathbf{H}}^\sigma) \begin{Bmatrix} \widehat{\chi}_{N_{\text{lay}}} \\ \widehat{\chi}_{N_{\text{lay}}-1} \\ \vdots \\ \widehat{\chi}_1 \end{Bmatrix} \right) = 0 \tag{A3}$$

Unknown stress parameters for all layers of the cross-section may be then obtained as (see (A3))

$$\{\widehat{\chi}_{N_{\text{lay}}}, \widehat{\chi}_{N_{\text{lay}}-1}, \ldots, \widehat{\chi}_1\}^T = (\widehat{\mathbf{H}}^\sigma)^{-1} \widehat{\mathbf{H}}^u \mathbf{U} \tag{A4}$$

Structure of $\widehat{\mathbf{H}}^\sigma$ and $\widehat{\mathbf{H}}^u$ is discussed in detail in the next section.

A.2. Matrices $(\widehat{\mathbf{H}}^\sigma)^{-1}$ and $\widehat{\mathbf{H}}^u$ for a three-layer case

In what follows, a procedure of getting $(\widehat{\mathbf{H}}^\sigma)^{-1}$ and $\widehat{\mathbf{H}}^u$ is explained in detail on example of three-layered laminate. Let us first write $\mathbf{H}_K^\sigma$ (see (47)) as

$$\mathbf{H}_K^\sigma = \begin{bmatrix} [tt]_K & [tR]_K & [tb]_K \\ [Rt]_K & [RR]_K & [Rb]_K \\ [bt]_K & [bR]_K & [bb]_K \end{bmatrix}_{(6\times6)} \tag{A5}$$

where top, resultant and bottom values are given in the form of (2×2) matrices. Next, $\widetilde{\mathbf{H}}^\sigma$ for three layers is constructed as explained in Section 4.2. Reduced matrix $\widehat{\mathbf{H}}^\sigma$ is obtained: (i) by eliminating the first 2 rows and the first 2 columns of (50); (ii) by eliminating the last 2 rows and the last 2 columns of (50); (iii) by moving sub-matrices along the diagonal. These modifications are done to satisfy conditions (52). For the three-layer case we end with

$$\widehat{\mathbf{H}}^\sigma = \begin{bmatrix} [RR]_3 & [Rb]_3 & \mathbf{0} & \mathbf{0} & \mathbf{0} \\ [bR]_3 & [bb]_3 + [tt]_2 & [tR]_2 & [tb]_2 & \mathbf{0} \\ \mathbf{0} & [Rb]_2 & [RR]_2 & [Rt]_2 & \mathbf{0} \\ \mathbf{0} & [tb]_2 & [tR]_2 & [bb]_2 + [tt]_1 & [tR]_1 \\ \mathbf{0} & \mathbf{0} & \mathbf{0} & [Rt]_1 & [RR]_1 \end{bmatrix}_{(10\times10)} \tag{A6}$$

All the sub-matrices in (A6) are of (2×2). Finally, $\widehat{\mathbf{H}}^\sigma$ is inverted. It proves convenient to write inverted matrix as a collection of (2×2) matrices

$$(\widehat{\mathbf{H}}^\sigma)^{-1} = \begin{bmatrix} [\widehat{H}^{RR}]_3^3 & [\widehat{H}^{Rt}]_2^3 & [\widehat{H}^{RR}]_2^3 & [\widehat{H}^{Rt}]_1^3 & [\widehat{H}^{RR}]_1^3 \\ [\widehat{H}^{tR}]_3^2 & [\widehat{H}^{tt}]_3^2 & [\widehat{H}^{tR}]_2^2 & [\widehat{H}^{tt}]_1^2 & [\widehat{H}^{tR}]_1^2 \\ [\widehat{H}^{RR}]_3^2 & [\widehat{H}^{Rt}]_2^2 & [\widehat{H}^{RR}]_2^2 & [\widehat{H}^{Rt}]_1^2 & [\widehat{H}^{RR}]_1^2 \\ [\widehat{H}^{tR}]_3^1 & [\widehat{H}^{tt}]_2^1 & [\widehat{H}^{tR}]_2^1 & [\widehat{H}^{tt}]_1^1 & [\widehat{H}^{tR}]_1^1 \\ [\widehat{H}^{RR}]_3^1 & [\widehat{H}^{Rt}]_2^1 & [\widehat{H}^{RR}]_2^1 & [\widehat{H}^{Rt}]_2^1 & [\widehat{H}^{RR}]_1^1 \end{bmatrix}_{(10\times10)} \tag{A7}$$

$\widehat{\mathbf{H}}^u$ is obtained by imposing interlaminar conditions on $\widetilde{\mathbf{H}}^u$ (see (46) and Section 4.2). We get matrix of the form

$$\widehat{\mathbf{H}}^u = \begin{bmatrix} \mathbf{b}_0 + f'(\xi_3)\, \mathbf{b}_1 \\ \mathbf{0}_{(2\times7)} \\ \mathbf{b}_0 + f'(\xi_2)\, \mathbf{b}_1 \\ \mathbf{0}_{(2\times7)} \\ \mathbf{b}_0 + f'(\xi_1)\, \mathbf{b}_1 \end{bmatrix}_{(10\times7)} \tag{A8}$$

Now, $\{\widehat{\chi}_3, \widehat{\chi}_2, \widehat{\chi}_1\}^T$ may be expressed from (A4). Note, that in a general case $(\widehat{\mathbf{H}}^\sigma)^{-1}$ is a quadratic $(n \times n)$ matrix of dimensions $n = 4N_{\text{lay}} - 2$, while $\widehat{\mathbf{H}}^u$ is an $(n \times 7)$ matrix.

A.3. Transverse shear stress resultants

Let us use (71) to obtain vector of unknown stress parameters $\widehat{\chi}_K$, see (A1), of layer $K \in [1, N_{\text{lay}}]$. By using (12) we may get σ_K, where matrix $\mathbf{E}$ in (12) has to be modified in accordance to the number of stress parameters in vector $\widehat{\chi}_K$. By integration of σ_K through the layer thickness we get

$$\int_{h_K^-}^{h_K^+} \sigma_K \, \mu \, \mathrm{d}\xi_K = \left(\int_{h_K^-}^{h_K^+} \widehat{\mathbf{E}} \, \mu \, \mathrm{d}\xi_K \right) \widehat{\chi}_K \stackrel{\mu=1}{=} \sum_{K^*}^{N_{\text{lay}}} [\widehat{H}^{RR}]_{K^*}^K (\mathbf{b}_0 + f'(\xi_{K^*}) \mathbf{b}_1) \mathbf{U} \tag{A9}$$

where $\widehat{\mathbf{E}}$ is modification of $\mathbf{E}$ defined in (13) (i.e. the columns related to non-appearing stress parameters in $\widehat{\chi}_K$ are dropped) and $[\widehat{H}^{RR}]_{K^*}^K$ are sub-matrices of dimensions (2×2) coming from (A7). By using the following notation:

$$\mathbf{Q}_K^0 = \sum_{K^*=1}^{N_{\text{lay}}} [\widehat{H}^{RR}]_{K^*}^K, \quad \mathbf{Q}_K^1 = \sum_{K^*=1}^{N_{\text{lay}}} f'(\xi_{K^*}) [\widehat{H}^{RR}]_{K^*}^K \tag{A10}$$

we can rewrite (A9) in the form of Equation (53):

$$\int_{h_K^-}^{h_K^+} \sigma_K \mu \, \mathrm{d}\xi_K = (\mathbf{Q}_K^0 \mathbf{b}_0 + \mathbf{Q}_K^1 \mathbf{b}_1) \mathbf{U} = \mathbf{Q}_K^0 \left\{ \begin{array}{c} \gamma_{13} \\ \gamma_{23} \end{array} \right\} + \mathbf{Q}_K^1 \left\{ \begin{array}{c} \gamma_{13}^f \\ \gamma_{23}^f \end{array} \right\} \tag{A11}$$

and thus relate stress resultants (obtained by through-thickness integration of continuous transverse stresses) with transverse strains.

APPENDIX B. STRAIN–DISPLACEMENT FINITE ELEMENT MATRICES

Starting from (16) and (19), the following discrete strain–displacement operator relative to the local Cartesian frame $\widehat{x}, \widehat{y}, \widehat{z}$ (see Section 5.2) is obtained

$$\varepsilon = \mathbf{B} \left\{ \begin{array}{c} \mathbf{U}_1 \\ \mathbf{U}_2 \\ \mathbf{U}_3 \\ \mathbf{U}_4 \end{array} \right\}, \quad \delta\varepsilon = \mathbf{B} \left\{ \begin{array}{c} \delta\mathbf{U}_1 \\ \delta\mathbf{U}_2 \\ \delta\mathbf{U}_3 \\ \delta\mathbf{U}_4 \end{array} \right\}, \quad \mathbf{B} = \begin{bmatrix} \mathbf{B}_m^1 & \mathbf{B}_m^2 & \mathbf{B}_m^3 & \mathbf{B}_m^4 \\ \mathbf{B}_b^1 & \mathbf{B}_b^2 & \mathbf{B}_b^3 & \mathbf{B}_b^4 \\ \mathbf{B}_s^1 & \mathbf{B}_s^2 & \mathbf{B}_s^3 & \mathbf{B}_s^4 \\ \mathbf{B}_b^{f,1} & \mathbf{B}_b^{f,2} & \mathbf{B}_b^{f,3} & \mathbf{B}_b^{f,4} \\ \mathbf{B}_s^{f,1} & \mathbf{B}_s^{f,2} & \mathbf{B}_s^{f,3} & \mathbf{B}_s^{f,4} \end{bmatrix}_{(13 \times 28)} \tag{B1}$$

Vectors ε and $\mathbf{U}$ are given in (35)$_2$ and (7). The membrane part related to the node 'I' may be expressed as

$$\mathbf{B}_m^I = \begin{bmatrix} N_{,\widehat{x}}^I (\mathbf{X}_{,\widehat{x}}^0)^{\mathrm{T}} & \mathbf{0}_{(1 \times 2)} & \mathbf{0}_{(1 \times 2)} \\ N_{,\widehat{y}}^I (\mathbf{X}_{,\widehat{y}}^0)^{\mathrm{T}} & \mathbf{0}_{(1 \times 2)} & \mathbf{0}_{(1 \times 2)} \\ N_{,\widehat{x}}^I (\mathbf{X}_{,\widehat{y}}^0)^{\mathrm{T}} + N_{,\widehat{y}}^I (\mathbf{X}_{,\widehat{x}}^0)^{\mathrm{T}} & \mathbf{0}_{(1 \times 2)} & \mathbf{0}_{(1 \times 2)} \end{bmatrix}_{(3 \times 7)} \tag{B2}$$

while the bending part (due to the linear distribution of displacements through the thickness) related to the node 'I' takes the form

$$\mathbf{B}_b^I = \begin{bmatrix} \mathbf{0}_{(1\times3)} & N_{,\hat{x}}^I(\mathbf{X}_{,\hat{x}}^0)^{\mathrm{T}}\mathbf{\Lambda}_I & \mathbf{0}_{(1\times2)} \\ \mathbf{0}_{(1\times3)} & N_{,\hat{y}}^I(\mathbf{X}_{,\hat{y}}^0)^{\mathrm{T}}\mathbf{\Lambda}_I & \mathbf{0}_{(1\times2)} \\ \mathbf{0}_{(1\times3)} & (N_{,\hat{x}}^I(\mathbf{X}_{,\hat{y}}^0)^{\mathrm{T}} + N_{,\hat{y}}^I(\mathbf{X}_{,\hat{x}}^0)^{\mathrm{T}})\mathbf{\Lambda}_I & \mathbf{0}_{(1\times2)} \end{bmatrix}_{(3\times7)} \tag{B3}$$

In accordance with the ANS approach, the transverse shear part (due to the linear distribution of displacements through the thickness) of (B1) is

$$\mathbf{B}_s = [\mathbf{B}_s^1, \mathbf{B}_s^2, \mathbf{B}_s^3, \mathbf{B}_s^4] = \begin{bmatrix} \mathbf{B}_{s\hat{x}}^1 & \mathbf{B}_{s\hat{x}}^2 & \mathbf{B}_{s\hat{x}}^3 & \mathbf{B}_{s\hat{x}}^4 \\ \mathbf{B}_{s\hat{y}}^1 & \mathbf{B}_{s\hat{y}}^2 & \mathbf{B}_{s\hat{y}}^3 & \mathbf{B}_{s\hat{y}}^4 \end{bmatrix}_{(2\times28)} \tag{B4}$$

where the following transformation (see (61)) is applied:

$$\mathbf{B}_{s\hat{x}}^I = \frac{\partial\xi}{\partial\hat{x}}\mathbf{B}_{s\xi}^I + \frac{\partial\eta}{\partial\hat{x}}\mathbf{B}_{s\eta}^I, \quad \mathbf{B}_{s\hat{x}}^I = \frac{\partial\xi}{\partial\hat{y}}\mathbf{B}_{s\xi}^I + \frac{\partial\eta}{\partial\hat{y}}\mathbf{B}_{s\eta}^I \tag{B5}$$

The transverse shear part of the operator in the direction of ξ is

$$\mathbf{B}_{s\xi}^1 = \tfrac{1}{4}(1-\eta)[-(\mathbf{T}_A)^{\mathrm{T}} \mid (\mathbf{X}_{A,\xi}^0)^{\mathrm{T}}\mathbf{\Lambda}_1 \mid \mathbf{0}_{(1\times2)}]_{(1\times7)}$$

$$\mathbf{B}_{s\xi}^2 = \tfrac{1}{4}(1-\eta)[(\mathbf{T}_A)^{\mathrm{T}} \mid (\mathbf{X}_{A,\xi}^0)^{\mathrm{T}}\mathbf{\Lambda}_2 \mid \mathbf{0}_{(1\times2)}]_{(1\times7)}$$

$$\mathbf{B}_{s\xi}^3 = \tfrac{1}{4}(1+\eta)[(\mathbf{T}_C)^{\mathrm{T}} \mid (\mathbf{X}_{C,\xi}^0)^{\mathrm{T}}\mathbf{\Lambda}_3 \mid \mathbf{0}_{(1\times2)}]_{(1\times7)}$$

$$\mathbf{B}_{s\xi}^4 = \tfrac{1}{4}(1+\eta)[-(\mathbf{T}_C)^{\mathrm{T}} \mid (\mathbf{X}_{C,\xi}^0)^{\mathrm{T}}\mathbf{\Lambda}_4 \mid \mathbf{0}_{(1\times2)}]_{(1\times7)} \tag{B6}$$

and in the direction of η

$$\mathbf{B}_{s\eta}^1 = \tfrac{1}{4}(1-\xi)[-(\mathbf{T}_D)^{\mathrm{T}} \mid (\mathbf{X}_{D,\eta}^0)^{\mathrm{T}}\mathbf{\Lambda}_1 \mid \mathbf{0}_{(1\times2)}]_{(1\times7)}$$

$$\mathbf{B}_{s\eta}^2 = \tfrac{1}{4}(1+\xi)[-(\mathbf{T}_B)^{\mathrm{T}} \mid (\mathbf{X}_{B,\eta}^0)^{\mathrm{T}}\mathbf{\Lambda}_2 \mid \mathbf{0}_{(1\times2)}]_{(1\times7)}$$

$$\mathbf{B}_{s\eta}^3 = \tfrac{1}{4}(1+\xi)[(\mathbf{T}_B)^{\mathrm{T}} \mid (\mathbf{X}_{C,\eta}^0)^{\mathrm{T}}\mathbf{\Lambda}_3 \mid \mathbf{0}_{(1\times2)}]_{(1\times7)}$$

$$\mathbf{B}_{s\eta}^4 = \tfrac{1}{4}(1-\xi)[(\mathbf{T}_D)^{\mathrm{T}} \mid (\mathbf{X}_{C,\eta}^0)^{\mathrm{T}}\mathbf{\Lambda}_4 \mid \mathbf{0}_{(1\times2)}]_{(1\times7)} \tag{B7}$$

The ξ and η derivatives of middle surface position vector at the points A, B, C, D are

$$\mathbf{X}_{A,\xi}^0 = \tfrac{1}{2}(\mathbf{X}_2^0 - \mathbf{X}_1^0), \quad \mathbf{X}_{C,\xi}^0 = \tfrac{1}{2}(\mathbf{X}_3^0 - \mathbf{X}_4^0)$$

$$\mathbf{X}_{B,\eta}^0 = \tfrac{1}{2}(\mathbf{X}_3^0 - \mathbf{X}_2^0), \quad \mathbf{X}_{D,\eta}^0 = \tfrac{1}{2}(\mathbf{X}_4^0 - \mathbf{X}_1^0) \tag{B8}$$

while the position of shell director at the points A, B, C, D may be obtained as

$$\mathbf{T}_A = \tfrac{1}{2}(\mathbf{T}_2 + \mathbf{T}_1), \quad \mathbf{T}_C = \tfrac{1}{2}(\mathbf{T}_3 + \mathbf{T}_4)$$

$$\mathbf{T}_B = \tfrac{1}{2}(\mathbf{T}_3 + \mathbf{T}_2), \quad \mathbf{T}_D = \tfrac{1}{2}(\mathbf{T}_4 + \mathbf{T}_1) \tag{B9}$$

The bending part of the discrete strain–displacement operator which appears due to the zig-zag-shaped function may be for the node 'I' expressed as

$$\mathbf{B}_b^{f,I} = \begin{bmatrix} \mathbf{0}_{(1\times3)} & \mathbf{0}_{(1\times2)} & N_{,\hat{x}}^I(\mathbf{X}_{,\hat{x}}^0)^T\widetilde{\mathbf{Q}}_I \\ \mathbf{0}_{(1\times3)} & \mathbf{0}_{(1\times2)} & N_{,\hat{y}}^I(\mathbf{X}_{,\hat{y}}^0)^T\widetilde{\mathbf{Q}}_I \\ \mathbf{0}_{(1\times3)} & \mathbf{0}_{(1\times2)} & (N_{,\hat{x}}^I(\mathbf{X}_{,\hat{y}}^0)^T + N_{,\hat{y}}^I(\mathbf{X}_{,\hat{x}}^0)^T)\widetilde{\mathbf{Q}}_I \end{bmatrix}_{(3\times7)} \tag{B10}$$

The transverse shear part of the discrete strain–displacement operator which appears due to the zig-zag-shaped function may be, in accordance with ANS approach, expressed as

$$\mathbf{B}_s^f = [\mathbf{B}_s^{f,1}, \mathbf{B}_s^{f,2}, \mathbf{B}_s^{f,3}, \mathbf{B}_s^{f,4}] = \begin{bmatrix} \mathbf{B}_{s\hat{x}}^{f,1} & \mathbf{B}_{s\hat{x}}^{f,2} & \mathbf{B}_{s\hat{x}}^{f,3} & \mathbf{B}_{s\hat{x}}^{f,4} \\ \mathbf{B}_{s\hat{y}}^{f,1} & \mathbf{B}_{s\hat{y}}^{f,2} & \mathbf{B}_{s\hat{y}}^{f,3} & \mathbf{B}_{s\hat{y}}^{f,4} \end{bmatrix}_{(2\times28)} \tag{B11}$$

where the same transformation as in (B5) is applied

$$\mathbf{B}_{s\hat{x}}^{f,I} = \frac{\partial\xi}{\partial\hat{x}}\mathbf{B}_{s\xi}^{f,I} + \frac{\partial\eta}{\partial\hat{x}}\mathbf{B}_{s\eta}^{f,I}, \quad \mathbf{B}_{s\hat{x}}^{f,I} = \frac{\partial\xi}{\partial\hat{y}}\mathbf{B}_{s\xi}^{f,I} + \frac{\partial\eta}{\partial\hat{y}}\mathbf{B}_{s\eta}^{f,I} \tag{B12}$$

The zig-zag transverse shear part of the discrete strain–displacement operator in the direction of ξ is

$$\mathbf{B}_{s\xi}^{f,1} = \tfrac{1}{4}(1-\eta)[\mathbf{0}_{(1\times3)}\,|\,\mathbf{0}_{(1\times2)}\,|\,(\mathbf{X}_{A,\xi}^0)^T\widetilde{\mathbf{Q}}_1]_{(1\times7)}$$

$$\mathbf{B}_{s\xi}^{f,2} = \tfrac{1}{4}(1-\eta)[\mathbf{0}_{(1\times3)}\,|\,\mathbf{0}_{(1\times2)}\,|\,(\mathbf{X}_{A,\xi}^0)^T\widetilde{\mathbf{Q}}_2]_{(1\times7)}$$

$$\mathbf{B}_{s\xi}^{f,3} = \tfrac{1}{4}(1+\eta)[\mathbf{0}_{(1\times3)}\,|\,\mathbf{0}_{(1\times2)}\,|\,(\mathbf{X}_{C,\xi}^0)^T\widetilde{\mathbf{Q}}_3]_{(1\times7)} \tag{B13}$$

$$\mathbf{B}_{s\xi}^{f,4} = \tfrac{1}{4}(1+\eta)[\mathbf{0}_{(1\times3)}\,|\,\mathbf{0}_{(1\times2)}\,|\,(\mathbf{X}_{C,\xi}^0)^T\widetilde{\mathbf{Q}}_4]_{(1\times7)}$$

while the zig-zag transverse shear part of the discrete strain–displacement operator in the direction of η is

$$\mathbf{B}_{s\eta}^{f,1} = \tfrac{1}{4}(1-\xi)[\mathbf{0}_{(1\times3)}\,|\,\mathbf{0}_{(1\times2)}\,|\,(\mathbf{X}_{D,\eta}^0)^T\widetilde{\mathbf{Q}}_1]_{(1\times7)}$$

$$\mathbf{B}_{s\eta}^{f,2} = \tfrac{1}{4}(1+\xi)[\mathbf{0}_{(1\times3)}\,|\,\mathbf{0}_{(1\times2)}\,|\,(\mathbf{X}_{B,\eta}^0)^T\widetilde{\mathbf{Q}}_2]_{(1\times7)}$$

$$\mathbf{B}_{s\eta}^{f,3} = \tfrac{1}{4}(1+\xi)[\mathbf{0}_{(1\times3)}\,|\,\mathbf{0}_{(1\times2)}\,|\,(\mathbf{X}_{C,\eta}^0)^T\widetilde{\mathbf{Q}}_3]_{(1\times7)} \tag{B14}$$

$$\mathbf{B}_{s\eta}^{f,4} = \tfrac{1}{4}(1-\xi)[\mathbf{0}_{(1\times3)}\,|\,\mathbf{0}_{(1\times2)}\,|\,(\mathbf{X}_{C,\eta}^0)^T\widetilde{\mathbf{Q}}_4]_{(1\times7)}$$

Note, that $\mathbf{B}_s$ is a discrete version of $\mathbf{b}_0$ matrix and $\mathbf{B}_s^f$ is a discrete version of $\mathbf{b}_1$ matrix in (44).

REFERENCES

1. Noor AK, Rarig PL. Three-dimensional solutions of laminated cylinders. *Computer Methods in Applied Mechanics and Engineering* 1974; 3:319–334.
2. Ren JG. Exact solutions for laminated cylindrical shells in cylindrical bending. *Composite Science and Technology* 1987; 29:169–187.
3. Varadan TK, Bhaskar K. Bending of laminated orthotropic cylindrical shells—an elasticity approach. *Composite Structures* 1991; 17:141–156.

4. Carrera E. A class of two dimensional theories for multilayered plates analysis. *Atti Accademia delle Scienze di Torino, Mem Sci. Fis.* 1995; **19–20**:49–87.
5. Carrera E. C_z^0 requirements—models for the two dimensional analysis of multilayered structures. *Composite Structures* 1997; **37**:373–384.
6. Srinivas S. A refined analysis of composite laminates. *Journal of Sound and Vibration* 1973; **30**:495–50?.
7. Reddy JN. On refined computational models of composite laminates. *International Journal for Numerical Methods in Engineering* 1989; **27**:362–382.
8. Carrera E. Multilayered shell theories accounting for a layer-wise mixed description. Part I. Governing equations. Part II Numerical evaluations. *American Journal of Aeronautics and Astronautics* 1999; **37**:1107–1124.
9. Ren JG. A new theory for laminated plates. *Composite Science and Technology* 1986; **26**:225–239.
10. Murakami H. Laminated composite plate theory with improved in-plane response. *Journal of Applied Mechanics* 1986; **53**:661–666.
11. Librescu L. Refined geometrically non-linear theories of anisotropic laminated shells. *Quarterly of Applied Mathematics* 1987; **55**:1–22.
12. Grigolyuk EI, Kulikov GM. General direction of the development of the theory of shells. *Mekhanica Kompozitnykh Materialov* 1988; **2**:287–298.
13. Kapania RK, Raciti S. Recent advances in analysis of laminated beams and plates, Part I: Shear effects and buckling. *AIAA Journal* 1989; **27**:923–934.
14. Kapania RK. A review on the analysis of laminated shells. *Journal of Pressure Vessel Technology* 1989; **111**:88–96.
15. Noor AK, Burton WS. Assessment of computational models for multilayered composite shells. *Applied Mechanics Review* 1990; **43**:67–97.
16. Noor AK, Burton S, Bert CW. Computational model for sandwich panels and shells. *Applied Mechanics Review* 1996; **49**:155–199.
17. Palazotto AN, Dennis ST. Nonlinear Analysis of Shell Structures. *AIAA Series*, 1992.
18. Basar Y, Ding Y, Shultz R. Refined shear deformation models for composite laminates with finite rotation. *International Journal of Solids and Structures* 1993; **30**:2611–2638.
19. Di S, Ramm E. Hybrid stress formulation for higher-order theory of laminated shell analysis. *Computer Methods in Applied Mechanics and Engineering* 1993; **109**:359–376.
20. Pinsky PM, Kim KO. A multidirector formulation for elastic–viscoelastic layered shells. *International Journal for Numerical Methods in Engineering* 1986; **23**:2213–2244.
21. Braun M, Bischoff M, Ramm E. Nonlinear shell formulation for complete three-dimensional constitutive laws including composites and laminates. *Computational Mechanics* 1994; **15**:1–18.
22. Gruttmann F, Wagner W, Meyer L, Wriggers P. A nonlinear composite shell elements with continuous interlaminar shear stress. *Computational Mechanics* 199?; **13**:175–188.
23. Reissner E. On a certain mixed variational theory and a proposed applications. *International Journal for Numerical Methods in Engineering* 1984; **20**:1366–1368.
24. Carrera E. C^0 Reissner–Mindlin multilayered plate elements including zig-zag and interlaminar stresses continuity. *International Journal of Numerical Methods in Engineering* 1996; **39**:1797–1820.
25. Carrera E, Kröplin, B. Zig-zag and interlaminar equilibria effects in large deflection and postbuckling analysis of multilayered plates. *Mechanics of Composite Materials and Structures* 1997; **4**:69–94.
26. Bhaskar K, Varadan TK. Reissner's new mixed variational principle applied to laminated cylindrical shells. *Journal of Pressure Vessel Technology* 1992; **114**:115–119.
27. Ibrahimbegović A, Brank B, Courtois P. Constrained finite rotations vector-like parameters for geometrically exact shells. In *Proceedings of European Conference On Computational Mechanics* 1999; 285–298.
28. Jones RM. *Mechanics of Composite Materials*. McGraw-Hill: New York, 1975.
29. Carrera E. A refined multilayered finite element model applied to linear and nonlinear analysis of sandwich structures. *Composite Science and Technology* 1998; **58**:1553–1569.
30. Brank B, Perić D, Damjanić FB. On the implementation of a nonlinear four node shell element for thin multilayered elastic shells. *Computational Mechanics* 1995; **16**:341–359.
31. Bathe KJ, Dvorkin EN. A four node plate bending element based on Mindlin/Reissner plate theory and mixed interpolation. *International Journal for Numerical Methods in Engineering* 1985; **21**:367–383.
32. Pagano JN, Hatfield SJ. Elastic behavior of multilayered bidirectional composites. *AIAA Journal* 1972; **10**:931–933.
33. Pandya BN, Kant T. A refined higher-order generally orthotropic C^0 plate bending elements. *Computers and Structures* 1988; **28**:119–133.
34. Noor AK, Peters WS. A posteriori estimates for shear correction factors in multilayered composite cylinders. *Journal of Engineering Mechanics* 1989; **115**:1225–1245.
35. Carrera E. A study of transverse normal stress effect on vibration of multilayered plates and shells. *Journal of Sound and Vibration* 1999; **225**:803–829.
36. Dennis ST, Palazotto AN. Laminated shell in cylindrical bending, two-dimensional approach vs exact. *AIAA Journal* 1991; **29**:647–650.
37. Kant T, Khare RK. A higher-order facet quadrilateral composite shell element. *International Journal for Numerical Methods in Engineering* 1997; **40**:4477–4499.

38. Jing H, Tzeng K. Refined shear deformation theory of laminated shells. *AIAA Journal* 1993; **31**:765–773.
39. Liou WJ, Sun CT. A three-dimensional hybrid stress isoparametric element for the analysis of laminated composite plates. *Computers and Structures* 1987; **25**:241–249.
40. Reddy JN. A simple higher order theory for laminated composite plates. *Journal of Applied Mechanics* 1984; **51**: 745–752.
41. Carrera E, Parisch H. Evaluation of geometrical nonlinear effects of thin and moderately thick multilayered composite shells. *Composite Structures* 1998; **40**:11–24.
42. Bhaskar K, Varadan TK. A higher-order theory for bending analysis of laminated shells of revolution. *Computers and Structures* 1991; **40**:815–819.